NASA Technical Paper 1558

Hydroelastic Vibration Analysis of Partially Liquid-Filled Shells Using a Series Representation of the Liquid

Jerrold M. Housner, Robert W. Herr,
and John L. Sewall

MARCH 1980

NASA

NASA Technical Paper 1558

Hydroelastic Vibration Analysis of Partially Liquid-Filled Shells Using a Series Representation of the Liquid

Jerrold M. Housner, Robert W. Herr,
and John L. Sewall
Langley Research Center
Hampton, Virginia

National Aeronautics
and Space Administration

**Scientific and Technical
Information Office**

1980

A

SUMMARY

A series representation of the oscillatory behavior of incompressible nonviscous liquids contained in partially filled elastic tanks is presented. By selecting each term of the series on the basis of the hydroelastic vibrations in circular cylindrical tanks, each term satisfies the governing liquid equation (Laplace's equation) but does not satisfy the liquid-tank interface compatibility. By using a complementary energy principle presented herein, the superposition of these terms is made to approximately satisfy the interface compatibility. This analysis is applied to the gravity sloshing and hydroelastic vibrations of liquids in hemispherical tanks and in a typical elastic aerospace propellant tank. With only a few series terms being retained, the results correlated very well with existing analytical results, NASTRAN[1]-generated analytical results, and experimental test results. Hence, although each term is based on a cylindrical tank geometry, the superposition can be successfully applied to noncylindrical tanks.

INTRODUCTION

Liquid-fuel tanks are often large components of aerospace vehicles and significantly affect the vibratory behavior of an entire vehicle. In turn, the motions of liquid in a fuel tank can be expected to play a significant role in tank vibrations. Consequently, vibration analyses of such tanks must include interactive coupling between the elastic shell tank structure and the contained liquid.

Early analytical investigations of liquid-tank vibrations were mostly limited to simple tank geometries, such as circular cylinders. A thorough survey of these early investigations is given in reference 1, chapter 9. More recently, computer programs have been developed which treat the liquid-tank interaction problem in more general tank geometries found in practice. (See, for example, refs. 2 to 7.) The procedure used in these references to develop such programs was to modify existing shell programs to include liquid-structure interaction. The key element in these interaction analyses is the selection of a suitable representation of the liquid oscillatory behavior.

Since modeling the shell tank alone may require many degrees of freedom, a liquid model which introduces a minimum number of additional degrees of freedom is desirable. In references 2 to 5, finite-element models of the liquid are employed. Such models introduce a large number of degrees of freedom into the interaction problem since, in general, a three-dimensional body of liquid must be modeled. Furthermore, the distribution of finite elements throughout the liquid may pose modeling problems. In reference 6, the liquid is represented by a distribution of simple sources on the surface of the liquid. With this

---

[1]Registered trademark of the National Aeronautics and Space Administration.

approach, only the liquid surface is discretized and, consequently, the number of degrees of freedom is drastically reduced from the number introduced by the finite-element approach. In reference 7, the liquid model involves a series representation of the liquid oscillatory pressure with the liquid considered incompressible and gravity surface effects neglected. In this model, the degrees of freedom are the amplitude coefficients of terms of the series. The series is chosen so that each term exactly satisfies the governing equation for the behavior of the liquid (Laplace's equation). Using a series composed of these terms in a complementary energy principle for the liquid produces surface-integral governing equations. Thus, as in reference 6, only the liquid surface is discretized for numerical solution of these equations. Furthermore, the individual terms of the series capture the essence of the liquid behavior; consequently, the total number of degrees of freedom required for the coupled liquid-shell interaction problem is only slightly greater than that required for the empty shell. In addition, this approach can be applied successfully to a wide variety of shell geometrical shapes.

Inasmuch as the pressure-series representation provides accurate solutions when gravity effects are neglected, it is reasonable to anticipate that the approach can be successfully extended to include such effects. The inclusion of gravity permits the analysis to be applied to the physically important sloshing modes of the liquid which occur with little or no interaction with the elastic tank.

The purpose of the present paper is to extend the analysis of reference 7 to include gravity effects in the liquid. Further, since the analysis and application to incompressible liquids were only briefly described in reference 7, a more thorough description is presented herein. A series representation of the liquid oscillatory pressure is employed in a complementary energy principle which is derived herein for incompressible liquids in the presence of gravity. The terms of the series are uniquely selected to satisfy the governing liquid equation. Then, as in reference 7, the liquid pressure loading on the tank wall which depends on the wall deformation may be calculated without further discretization of the liquid. The deformation-dependent pressure of the liquid on the tank wall then becomes a loading term in the shell equations, and existing shell computer programs may be easily modified to accommodate this loading. In the present paper, the modification of the shell-of-revolution program of references 8 and 10 is discussed.

Applications of the modified shell program are presented for the following problems: liquid sloshing in a rigid hemisphere, hydroelastic vibrations of an incompressible liquid in an elastic propellant tank, and hydroelastic vibrations of an incompressible liquid in an elastic hemisphere. Furthermore, the convergence of the series expansion is considered in each application, and the results are compared with experiment and with NASTRAN analyses to validate the approach. Appendixes to the report provide a proof for the complementary energy principle used herein and descriptions of the NASTRAN analysis and experiment.

SYMBOLS

a	radius of hemisphere
$\hat{A}_1, \hat{A}_2, \hat{A}_3, A$	matrices whose elements are defined by equations (32) to (35)
b_m	mth amplitude coefficient of series expansion, see equations (8) and (9)
B, B', B''	matrices whose elements are defined in equations (51), (41), and (46), respectively
c_m	defined by equation (19)
C	diagonal matrix whose elements are c_m
$\tilde{F}$	column vector of forces from liquid acting on the wetted shell surface at I_ℓ nodal stations
$\tilde{g}, g$	gravitational vector in x-direction and magnitude, respectively
h	height of liquid
I_ℓ	number of nodal stations on wetted shell surface at which liquid pressures and forces are calculated
I_n	modified Bessel function of first kind of order n
j	$= \sqrt{-1}$
J_n	Bessel function of first kind of order n
K_n	modified Bessel function of second kind of order n
ℓ	length of tank in axial direction
m	number of half-waves along meridian
M	half the total number of terms in series expansion
M_ℓ	liquid apparent mass matrix
M_1, M_2, M_3	number of series terms associated with positive, negative, and zero values of λ_m, respectively
n	number of circumferential waves

n_x	component of $\tilde{N}$ in x-direction
$\tilde{N}$	outward unit vector normal to shell surface
p	liquid oscillatory compressive pressure
q_{mn}	mth series term in nth circumferential trigonometric harmonic
q^*_{mn}	series term defined in equation (61)
$Q, \hat{Q}_1, \hat{Q}_2$	matrices whose elements are found from equation (34)
r	radial coordinate shown in figure 1
R	value of r at shell wall
s	meridional coordinate of shell shown in figure 1
S_o	shell surface area
S_f, S_w	free and wetted shell surface, respectively, of liquid
t	time
T	transformation matrix defined by equation (51)
T_c	complementary kinetic energy of liquid
$\tilde{u}$	liquid displacement vector
u_x	component of $\tilde{u}$ in x-direction
$U_{c,g}$	gravitational energy
V_o	liquid volume
w	outward normal displacement of shell
W_c	complementary work of applied displacements
x	axial coordinate shown in figure 1
$\tilde{Y}$	position vector of liquid particle, equation (7)
Y_n	Bessel function of second kind of order n
Z_{mn}	defined in equation (17)

$\gamma_m^{(s)}, \gamma_m^{(c)}$ defined by equations (15) and (16), respectively

Γ gravitational load matrix defined by equation (53)

δ variational operator

δ_{ij} Kronecker delta function defined in equation (35)

η $= g/\omega^2 h$

η^* eigenvalue of equation (46)

θ circumferential coordinate shown in figure 1

λ_m mth value of selected parameter which determines type of series term to be used according to equations (14) to (17)

ρ_o mass density of liquid

σ_m defined by equation (20)

ϕ velocity potential for liquid

χ liquid load matrix defined by equation (52)

ψ angle between $\tilde{N}$ and r axis shown in figure 1

ω circular frequency

$\frac{\partial}{\partial N}$ derivative on shell wall parallel to $\tilde{N}$

A dot over a symbol denotes differentiation with respect to time.

A prime denotes differentiation with respect to x.

Bars over symbols refer to associated dimensionless quantities given by equation (27).

GENERAL THEORY FOR OSCILLATING LIQUID

Variational Principle

In appendix A, the following complementary energy principle is presented for a nonviscous incompressible liquid undergoing irrotational oscillations of the complex form $e^{j\omega t}$ about an initial compressed state:

$$\delta(T_c - U_{c,g} - W_c) = 0 \tag{1}$$

where the variations indicated by the operator δ are on all admissible pressure states, ω is the oscillatory circular frequency, j is $\sqrt{-1}$, and the variations of the complementary kinetic, gravitational, and external work energies are given by

$$\delta T_c = -\rho_o \int_{V_o} \nabla^2\phi \; \delta\phi \; dV_o + \rho_o \int_{S_o} \frac{\partial\phi}{\partial N} \; \delta\phi \; dS_o \tag{2}$$

$$\delta U_{c,g} = -\frac{g\rho_o}{j\omega} \int_{V_o} \nabla^2\phi \; \delta u_x \; dV_o - \frac{g\rho_o}{\omega^2} \int_{S_o} \frac{\partial\phi}{\partial N} \; \delta \frac{\partial\phi}{\partial N} \; n_x \; dS_o \tag{3}$$

$$\delta W_c = j\omega\rho_o \int_{S_w} \left[\delta\phi + \frac{g n_x}{\omega^2} \delta\left(\frac{\partial\phi}{\partial N}\right) \right] w \; dS_w \tag{4}$$

In equations (2) to (4), p is the oscillatory compressive pressure perturbation above the initial pressurized state P_o; ρ_o is the uniform mass density of the liquid; S_o and V_o are the liquid surface area and liquid volume, respectively; $\tilde{N}$ is a vector normal to S_o and positive outward; n_x is the component of $\tilde{N}$ in the positive x-direction (see fig. 1); $\tilde{g}$ is the gravity vector, which acts in the x-direction; S_w refers to the wetted portion of S_o; w is the shell displacement perturbation on S_w parallel to $\tilde{N}$; and ϕ is a velocity potential for the irrotational nonviscous liquid defined such that

$$\dot{\tilde{u}} = \text{grad } \phi \tag{5}$$

where the dot represents differentiation with respect to time and $\tilde{u}$ is tne liquid displacement vector.

The admissible pressure states for equation (1) must satisfy the free surface condition, namely $\delta_p = 0$ on S_f, the free surface portion of S_o; and the dynamic equilibrium of the liquid (or equivalently the linearized Bernoulli equation as established in appendix A), namely

$$p = \rho_o(-\dot{\phi} + \tilde{g} \cdot \tilde{u}) \tag{6}$$

Series Expansion

The velocity potential is approximated by a truncated series:

$$\phi(\tilde{Y}) = j\omega \sum_{m=1}^{2M} b_m \, q_m(\tilde{Y}) \tag{7}$$

where $\tilde{Y}$ is the position vector of a liquid particle. In equation (7) and henceforth, the complex multiplier $e^{j\omega t}$ is understood. Substituting equations (5) and (7) into equation (6) yields the series expansion for p,

$$p(\tilde{Y}) = \rho_o \sum_{m=1}^{2M} \left[\omega^2 \, q_m(\tilde{Y}) + g \, q_m'(\tilde{Y})\right] b_m \tag{8}$$

where the prime denotes differentiation with respect to x. Equations (7) and (8) may now be substituted into equations (2) to (4) and the results substituted into equation (1) to yield

$$\rho_o \int_{V_o} \sum_{m=1}^{2M} b_m \, \nabla^2 q_m \sum_{m=1}^{2M} \left(\omega^2 \, q_m + g \, q_m'\right) \delta b_m \, dV_o$$

$$- \rho_o \omega^2 \int_{S_w} \sum_{m=1}^{2M} b_m \frac{\partial q_m}{\partial N} \left[\sum_{m=1}^{2M} \left(q_m + \frac{g n_x}{\omega^2} \frac{\partial q_m}{\partial N}\right) \delta b_m\right] dS_w$$

$$+ \rho_o \omega^2 \int_{S_w} w \sum_{m=1}^{2M} \left(q_m + \frac{g n_x}{\omega^2} \frac{\partial q_m}{\partial N}\right) \delta b_m \, dS_w = 0 \tag{9}$$

where the effects of ullage volume have been neglected and the integral over S_f vanishes, since δp vanishes on S_f.

Since the numerical evaluation of the volume integral occurring in equation (9) can be a tedious task, it is desirable to cause this integral to vanish. This can be done by judiciously choosing q_m.

Selection of Series Terms

From the derivation of the complementary energy principle presented in appendix A, the volume integrand is equivalent to a statement of compatibility or incompressibility, namely

$$\nabla^2 \phi = 0 \tag{10}$$

Substituting equation (7) into equation (10) yields

$$\sum_{m=1}^{2M} \nabla^2 q_m \, b_m = 0 \tag{11}$$

Hence, compatibility is satisfied exactly and the volume integral vanishes exactly if q_m satisfies

$$\nabla^2 q_m = 0 \tag{12}$$

Equation (12) is a well-understood partial differential equation, and consequently the calculation of q_m for practical classes of problems is straightforward. In the next section, values of q_m are selected for liquids contained in arbitrarily shaped shell-of-revolution tanks.

As a consequence of equation (12), equation (9) becomes

$$\int_{S_w} \left(\sum_{m=1}^{2M} b_m \frac{\partial q_m}{\partial N} - w \right) \sum_{m=1}^{2M} \left(q_m + \frac{g n_x}{\omega^2} \frac{\partial q_m}{\partial N} \right) \delta b_m \, dS_w = 0 \tag{13}$$

Equation (13) is recognized as an approximate statement of the interface continuity between liquid and shell.

By selecting each series term on the basis of equation (12), each term captures a facet of the liquid behavior observed in classical liquid-shell vibration problems, such as periodically supported cylindrical shells containing incompressible liquid. (See also the discussion in ref. 7.) In other words, each term of the expansion may be viewed as being the exact modal pressure in a mode of some classical liquid-shell problem. The superposition of these terms is forced through equation (13) to approximately satisfy the liquid-shell interface condition of tank geometries radically different from the classical problem.

Liquids in Shells of Revolution

General Solution of Laplace's Equation

In many practical problems, the liquid is a body of revolution contained in a shell of revolution, as shown in figure 1. For such cases, each term of the series may be further expanded into trigonometric harmonics about the liquid circumference. The deformations of the shell may also be so expanded, and the expansion is uncoupled for each trigonometric harmonic. Then, all possible solutions of equation (12), when expressed in cylindrical coordinates, x, r, and θ, are the superposition of

$$q_{mn} = \begin{cases} Z_{mn}(r)\ \gamma_m^{(s)}(x) & (1 \leq m \leq M) \\ Z_{mn}(r)\ \gamma_m^{(c)}(x) & (M < m \leq 2M) \end{cases} \tag{14}$$

where the notation q_{mn} has been introduced to designate the coefficient of the nth harmonic and

$$\gamma_m^{(s)}(x) = \begin{cases} \sin\left(x\sqrt{\lambda_m}\right) & (\lambda_m > 0) \\ \sinh\left(x\sqrt{|\lambda_m|}\right) & (\lambda_m < 0) \\ x & (\lambda_m = 0) \end{cases} \tag{15}$$

$$\gamma_m^{(c)}(x) = \begin{cases} \cos\left(x\sqrt{\lambda_m}\right) & (\lambda_m > 0) \\ \cosh\left(x\sqrt{|\lambda_m|}\right) & (\lambda_m < 0) \\ 1 & (\lambda_m = 0) \end{cases} \tag{16}$$

$$Z_{mn}(r) = \begin{cases} \left.\begin{matrix} J_n\left(r\sqrt{|\lambda_m|}\right) \\ Y_n\left(r\sqrt{|\lambda_m|}\right) \end{matrix}\right\} & (\lambda_m < 0) \\ \left.\begin{matrix} I_n\left(r\sqrt{\lambda_m}\right) \\ K_n\left(r\sqrt{\lambda_m}\right) \end{matrix}\right\} & (\lambda_m > 0) \\ r^{\pm n} & (\lambda_m = 0) \end{cases} \tag{17}$$

where I_n, K_n, J_n, and Y_n are modified and unmodified Bessel functions of the first and second kinds, and for the present, it suffices to consider λ_m arbitrary. For nontoroidal shell-of-revolution tanks, the Bessel functions of the second kind, Y_n and K_n, and r^{-n} must be dropped since they are singular at the axis of revolution ($r = 0$).

Of course, the general solutions of equation (12) need not be expressed in cylindrical coordinates, that is, as cylindrical harmonics. For example, in tanks whose geometry more closely resembles spheres than cylinders, use of spherical coordinates should cause the pressure series expansion to converge more rapidly. Furthermore, if the liquid is outside of the tank, it is best to use spherical coordinates and hence spherical harmonics for q_{mn}. However, as is shown in the applications sections of this paper, cylindrical harmonics for q_{mn} provide accurate results for spherically shaped tanks with only a few terms being used. Further, the cylindrical formulation has the decided advantage that computer routines for Bessel functions are more widely available than routines for the associated Legendre polynomials required if spherical harmonics are used.

Satisfaction of Interface Continuity Relation (Eq. (13))

Substitution of equations (14) to (17) in equation (8) yields

$$p(x,r) = \rho_o \sum_{m=1}^{M} \left(\omega^2 b_m + g c_m b_{m+M}\right) \gamma_m^{(s)}(x)\ Z_{mn}(r)$$

$$+ \rho_o \sum_{m=1}^{M} \left(g\sigma_m b_m + \omega^2 b_{m+M}\right) \gamma_m^{(c)}(x)\ Z_{mn}(r) \qquad (18)$$

where

$$c_m = \begin{cases} -\sqrt{|\lambda_m|} & (\lambda_m > 0) \\ \sqrt{|\lambda_m|} & (\lambda_m < 0) \\ 0 & (\lambda_m = 0) \end{cases} \qquad (19)$$

$$\sigma_m = \begin{cases} \sqrt{|\lambda_m|} & (\lambda_m \neq 0) \\ 1 & (\lambda_m = 0) \end{cases} \tag{20}$$

Again, neglecting the effects due to ullage volume, $p = 0$ on the free surface ($x = 0$). Enforcing this condition yields from equation (18)

$$\sum_{m=1}^{M} \left(g\sigma_m b_m + \omega^2 b_{m+M}\right) Z_{mn}(r) = 0 \tag{21}$$

Inasmuch as equation (21) must hold for all r

$$b_{m+M} = -\frac{g\sigma_m}{\omega^2} b_m \tag{22}$$

Substituting equation (22) into equation (7) yields

$$\phi = j\omega \sum_{m=1}^{M} \left(q_{mn} - \frac{g\sigma_m}{\omega^2} q_{m+M}\right) b_m \tag{23}$$

Substituting equations (22) and (23) into equation (6) and using the Tong hypothesis of equation (A18) yields the oscillatory pressure,

$$p = \rho_o \omega^2 \sum_{m=1}^{M} \left[q_{mn} - \frac{g\sigma_m}{\omega^2} q_{m+M,n} + \frac{gn_x}{\omega^2}\left(\frac{\partial q_{mn}}{\partial N} - \frac{g\sigma_m}{\omega^2}\frac{\partial q_{m+M}}{\partial N}\right)\right] b_m \tag{24}$$

Finally, substituting equation (22) into equation (13) yields

$$\int_{S_w} \left\{ \left[\sum_{m=1}^{M} \left(\frac{\partial q_{mn}}{\partial N} - \frac{g\sigma_m}{\omega^2}\frac{\partial q_{m+M,n}}{\partial N}\right) b_m - w \right] \sum_{k=1}^{M} \left[q_{kn} - \frac{g\sigma_k}{\omega^2} q_{k+M,n} \right.\right.$$

$$\left.\left. + \frac{gn_x}{\omega^2}\left(\frac{\partial q_{kn}}{\partial N} - \frac{g\sigma_k}{\omega^2}\frac{\partial q_{k+M}}{\partial N}\right)\right] \delta b_k \right\} dS_w = 0 \tag{25}$$

Since equation (25) holds for all variations of b_k,

$$\int_{S_w} \left[\sum_{m=1}^{M} \left(\frac{\partial q_{mn}}{\partial N} - \frac{g\sigma_m}{\omega^2} \frac{\partial q_{m+M,n}}{\partial N} \right) b_m - w \right] \left[q_{kn} - \frac{g\sigma_k}{\omega^2} q_{k+M,n} \right.$$

$$\left. + \frac{gn_x}{\omega^2} \frac{\partial q_{kn}}{\partial N} - \left(\frac{g}{\omega^2} \right)^2 n_x \sigma_k \frac{\partial q_{k+M,n}}{\partial N} \right] dS_w = 0 \tag{26}$$

The following relations nondimensionalize equation (26):

$$\bar{r} = r/h; \quad \bar{x} = x/h; \quad \bar{N} = N/h; \quad \bar{w} = w/h; \quad \bar{R} = R/h; \quad \bar{s} = s/h;$$

$$\bar{b}_m = b_m/h^2; \quad \bar{\lambda}_m = h^2\lambda_m; \quad \bar{\sigma}_m = h\sigma_m; \quad \bar{c}_m = hc_m; \quad \eta = g/h\omega^2 \tag{27}$$

where h is the liquid height, R is the value of r at the shell wall, and s is a meridional coordinate as shown in figure 1. Equation (26) now becomes

$$\int_{S_w} \left[\sum_{m=1}^{M} \bar{b}_m \left(\frac{\partial q_{mn}}{\partial \bar{N}} - \eta \bar{c}_m \frac{\partial q_{m+M,n}}{\partial \bar{N}} \right) - \bar{w} \right] \left[q_{kn} - \eta \left(\bar{\sigma}_k q_{k+M,n} - n_x \frac{\partial q_{kn}}{\partial \bar{N}} \right) \right.$$

$$\left. - \eta^2 n_x \bar{c}_k \frac{\partial q_{k+M,n}}{\partial \bar{N}} \right] \bar{R}(\bar{s})\, d\bar{s}(\bar{x}) = 0 \tag{28}$$

Following reference 7, w is discretized by assuming a linear interpolation of w between I_ℓ liquid nodal stations on the wetted shell wall. Then equation (28) may be expressed in matrix notation as

$$\left[A - \eta\hat{A}_1 - \eta^2\hat{A}_2 - \eta^3\hat{A}_3 \right] \{\bar{b}\} = \left[Q - \eta\hat{Q}_1 - \eta^2\hat{Q}_2 \right] \{\bar{w}\} \tag{29}$$

where the elements of A, $\hat{A}_1$, $\hat{A}_2$, and $\hat{A}_3$ are defined as

$$A_{km} = \int_0^{\bar{s}(1)} \frac{\partial q_{mn}}{\partial \bar{N}} q_{kn} \bar{R}\, d\bar{s} \tag{30}$$

$$\hat{A}_{1,km} = \int_0^{\bar{s}(1)} \left(\bar{\sigma}_m \frac{\partial q_{m+M,n}}{\partial \bar{N}} q_{kn} + \bar{\sigma}_k \frac{\partial q_{mn}}{\partial \bar{N}} q_{k+M,n} - n_x \frac{\partial q_{mn}}{\partial \bar{N}} \frac{\partial q_{kn}}{\partial \bar{N}} \right) \bar{R} \, d\bar{s} \tag{31}$$

$$\hat{A}_{2,km} = \int_0^{\bar{s}(1)} \left[-\bar{\sigma}_m \frac{\partial q_{m+M,n}}{\partial \bar{N}} \left(\bar{\sigma}_k q_{k+M,n} - n_x \frac{\partial q_{kn}}{\partial \bar{N}} \right) + n_x \bar{\sigma}_k \frac{\partial q_{mn}}{\partial \bar{N}} \frac{\partial q_{k+M,n}}{\partial \bar{N}} \right] \bar{R} \, d\bar{s} \tag{32}$$

$$\hat{A}_{3,km} = - \int_0^{\bar{s}(1)} \bar{\sigma}_k \bar{\sigma}_m n_x \frac{\partial q_{m+M,n}}{\partial \bar{N}} \frac{\partial q_{k+M,n}}{\partial \bar{N}} \bar{R} \, d\bar{s} \tag{33}$$

where $1 \leq k \leq M$ and $1 \leq m \leq M$. The elements of the matrix Q are derived as in reference 7 by discretizing the wetted shell wall as

$$Q_{ki} = \left(1 - \delta_{k,I_\ell}\right) \int_{\bar{x}_i}^{\bar{x}_{i+1}} \bar{R} \left(1 - \frac{\bar{x} - \bar{x}_i}{\bar{x}_{i+1} - \bar{x}_i} \right) q_{kn} \, d\bar{x} / \cos \psi + \left(1 - \delta_{i1}\right) \int_{\bar{x}_{i-1}}^{\bar{x}_i} \left(\frac{\bar{x} - \bar{x}_{i-1}}{\bar{x}_i - \bar{x}_{i-1}} \right) \bar{R} q_{kn} \, d\bar{x} / \cos \psi \tag{34}$$

where the Kronecker delta is

$$\delta_{ij} = \begin{cases} 0 & (i \neq j) \\ 1 & (i = j) \end{cases} \tag{35}$$

and ψ is the angle formed by $\tilde{N}$ and the positive r axis as shown in figure 1. Also, the notation $\{\bar{w}\}$ and $\{\bar{b}\}$ represent column vectors of discrete normal shell displacements and series amplitude coefficients, respectively.

The elements of $\hat{Q}_1$ and $\hat{Q}_2$ are found from equation (34) by replacing q_{kn} by $\left(\bar{\sigma}_k q_{k+M,n} - n_x \frac{\partial q_{kn}}{\partial \bar{N}} \right)$ and $\left(\bar{\sigma}_k n_x \frac{\partial q_{k+M,n}}{\partial \bar{N}} \right)$, respectively. In appendix B, A, $\hat{A}_1$, $\hat{A}_2$, and $\hat{A}_3$ are shown to be symmetric matrices.

Some insight into the behavior of equation (29) may be revealed by considering two limiting cases. In the first case when $\omega^2 \to 0$ (hydrostatics), equation (29) reduces to

$$\{\bar{b}\} = \frac{1}{\eta}\left[\hat{A}_3^{-1}\hat{Q}_2\right]\{\bar{w}\} \tag{36}$$

Substituting equation (36) into equation (24) gives the vector of pressures at each liquid nodal station on the wetted shell wall,

$$\{p\} = -\rho_o\left[K_\ell\right]\{\bar{w}\} \tag{37}$$

where K_ℓ is a gravitational stiffness matrix defined as

$$\left[K_\ell\right] = gh\left[B'\tau\hat{A}_3^{-1}\hat{Q}_2\right] \tag{38}$$

The elements of the matrix B and the diagonal matrix τ are

$$B'_{im} = \bar{\sigma}_m \frac{\partial q_{m+M}}{\partial \bar{N}}\left(\bar{x}_i, \bar{R}_i\right) \tag{39}$$

$$\tau_{ij} = \begin{cases} 0 & (i \neq j) \\ \bar{\sigma}_i & (i = j) \end{cases} \tag{40}$$

with $\bar{x}_i$ and $\bar{R}_i$ being the values of $\bar{x}$ and $\bar{r}$ on the shell wall at the ith liquid nodal station as discussed in reference 7. The negative sign in equation (37) appears because positive pressure indicates compression.

As a second limiting case, consider the high-frequency oscillations when $\omega^2 \to \infty$. Equation (29) then reduces to

$$\{\bar{b}\} = \left[A^{-1}Q\right]\{\bar{w}\} \tag{41}$$

Substituting equation (41) into equation (24) gives the vector of pressures at each liquid nodal station on the wetted shell wall,

$$\{p\} = \rho_o\omega^2\left[M_\ell\right]\{\bar{w}\} \tag{42}$$

where M_ℓ is a liquid apparent mass matrix defined as in reference 7 to be

$$\left[M_\ell\right] = \left[B''A^{-1}Q\right] \tag{43}$$

where the elements of B'' are

$$B''_{im} = q_{mn}\left(\bar{x}_i, \bar{R}_i\right) \tag{44}$$

In general, equation (29) may be solved for the amplitude coefficients as follows:

$$\{\bar{b}\} = \left[A - \eta\hat{A}_1 - \eta^2\hat{A}_2 - \eta^3\hat{A}_3\right]^{-1}\left[Q - \eta\hat{Q}_1 - \eta^2\hat{Q}_2\right]\{\bar{w}\} \tag{45}$$

provided $\eta = \eta^*$ where η^* is an eigenvalue of the transcendental equation,

$$\left[A\right]\{\bar{b}\} = \left[\eta^*\hat{A}_1 + \eta^{*2}\hat{A}_2 + \eta^{*3}\hat{A}_3\right]\{\bar{b}\} \tag{46}$$

Most of the eigenvalues of equation (46) provide the sloshing frequencies of the liquid in a rigid tank, that is, for $\bar{w} = 0$. Their evaluation is discussed in the applications section of this paper. However, equation (46) by itself can result in a set of extraneous eigenvalues. This can occur because the variational principle used herein and derived in appendix A requires that δp not be identically zero for all x and r. Usually, this poses no problem; however, since δp depends explicitly on the eigenvalue in this formulation, then eigenvalues which make δp vanish identically may exist. In other words, the roots of the second bracketed term in equation (28) show up as erroneous eigenvalues of equation (46). Such roots occur only when

$$n_x = 1 \quad \text{and} \quad \eta^2 = \frac{1}{\bar{\sigma}_m \bar{c}_m} \qquad (m = 1,2,\ldots,M) \tag{47}$$

Hence, erroneous eigenvalues can only appear when gravitational effects are included. These eigenvalues may be readily recognized from equation (47) under the rare circumstances in which they can occur.

Substituting equation (45) into equation (24) gives the pressures on the wetted shell wall as

$$\{p\} = \rho_o\omega^2\left[\chi\right]\{\bar{w}\} \tag{48}$$

where

$$[\chi] = [B]\left[A - \eta\hat{A}_1 - \eta^2\hat{A}_2 - \eta^3\hat{A}_3\right]^{-1}\left[Q - \eta\hat{Q}_1 - \eta^2\hat{Q}_2\right] \tag{49}$$

and the elements of $[B]$ are

$$B_{im} = \left(1 + \eta\bar{\sigma}_m \frac{\partial}{\partial\bar{N}}\right)\left[q_{mn}\left(\bar{x}_i, \bar{R}_i\right) - \eta q_{m+M,n}\left(\bar{x}_i, \bar{R}_i\right)\right]$$

The forces on the shell wall may also be calculated as

$$\{F\} = [T]^{-1}\{p\} = \rho_o\omega^2\left[T^{-1}\chi\right]\{\bar{w}\} \tag{50}$$

where as in reference 7,

$$[T] = \begin{bmatrix} \frac{1}{R_1\,\Delta s_1} & 0 & \cdot & \cdot & \cdot & 0 \\ 0 & \frac{1}{R_2\,\Delta s_2} & & & & 0 \\ \cdot & & \cdot & & & \cdot \\ \cdot & & & \cdot & & \cdot \\ \cdot & & & & \cdot & \cdot \\ 0 & 0 & \cdot & \cdot & \cdot & \frac{1}{R_{I_\ell}\,\Delta s_{I_\ell}} \end{bmatrix} \tag{51}$$

As a consequence of the Maxwell-Betti reciprocal theorem, the matrix product $T^{-1}\chi$ is symmetric.

Convergence of Pressure Series

The convergence properties of the pressure series is a critical subject. A general proof showing its convergence in a coupled hydroelastic problem is not available and may not be possible. However, it is possible to demonstrate its rapid convergence to accurate results through the use of examples. Such examples are presented in the applications section of this paper.

Hydroelastic Modes

Hydroelastic modes are those modes in which there is significant coupling of the liquid and shell motions. In contrast, slosh modes involve little or no shell motion. Previous authors have reported that gravity has little effect on the hydroelastic modes. (See ref. 1, ch. 9, and ref. 11, for example). In other words $\eta << 1$. Consequently, when searching for the hydroelastic modes, higher order terms in η may be dropped in equation (46), resulting in

$$[\chi] = [M_\ell] + \eta[\Gamma] \tag{52}$$

where

$$[\Gamma] = \left[BA^{-1}\right]\left[\hat{A}_1 A^{-1} Q - A^{-1}\hat{Q}_1\right] \tag{53}$$

Equations (48) and (50) may now be rewritten as

$$\{p\} = \left(\rho_o \omega^2 [M_\ell] + \frac{\rho_o g}{h}[\Gamma]\right)\{\bar{w}\} \tag{54}$$

$$\{F\} = \left(\rho_o \omega^2 \left[T^{-1} M_\ell\right] + \frac{\rho_o g}{h}\left[T^{-1}\Gamma\right]\right)\{\bar{w}\} \tag{55}$$

Equation (54) or (55) provides the wall-deformation-dependent loading terms in the shell equations.

MODIFIED SHELL EQUATIONS

Discretized Form

If the shell equations have been discretized, as they would be for a finite-element or finite-difference shell solution, the liquid loading is readily accounted for in the shell equations as,

$$0 = \begin{bmatrix} K_{uu} & K_{uw} \\ K_{uw}^T & K_{ww} - \frac{\rho_o g}{h} T^{-1}\Gamma \end{bmatrix} \begin{Bmatrix} \bar{U} \\ \bar{w} \end{Bmatrix} - \omega^2 \begin{bmatrix} M_{uu} & 0 \\ 0 & M_{ww} + \rho_o T^{-1} M_\ell \end{bmatrix} \begin{Bmatrix} \bar{U} \\ \bar{w} \end{Bmatrix} \tag{56}$$

where the K's refer to stiffness and the M's to mass and the dimensionless vector $\bar{U}$ includes tangential shell displacements as well as those radial ones not on the wetted shell surface; in deriving equation (56), the approximate hydroelastic liquid loading of equation (55) has been used. The eigenvalues and eigenvectors can be extracted from equation (56) by the standard procedures.

Differential Equation Form

In some existing computer programs for shell vibration analysis, the differential equations are solved by numerical integration. This is the case for the numerical analysis of references 8 to 10. This analysis and the associated computer program have been modified to incorporate the shell-wall-deformation-dependent liquid pressure loading developed in the previous section. The results presented in the applications section of this paper were generated from this modified shell-of-revolution program.

The program uses a generalized form of Novozhilov's shell equations which include the nonlinear case of moderate rotations. These equations are transformed into a set of eight first-order differential equations in eight basic force and displacement shell variables and are solved using a Zarghamee version of the forward integration method.

Among other features the program has branched shell capability and can account for effects of prestressing of the shell walls. The branched shell capability makes it possible to treat assemblies of tanks often found in practice. Prestress effects in shell walls, which effectively stiffen the tank, can result from initial pressurization of the tank or the weight of the liquid under gravity or other longitudinal acceleration. (Previous work for cylindrical shell structures, such as that in ref. 12, has shown that prestress effects can be important.)

The shell differential equations as presented in reference 8 are

$$r \frac{dy_n}{ds} + a_n(s)\, y_n - b_n(s)\, z_n = F_n(s) \tag{57}$$

$$r \frac{dz_n}{ds} - c_n(s)\, y_n + d_n(s)\, z_n = 0 \tag{58}$$

where s is a meridional coordinate. The force vector y_n, displacement vector z_n, and coefficient matrices a, b, c, and d are defined in the reference. In addition, the surface load vector $F_n(s)$ is given as

$$F_n(s) = \begin{Bmatrix} X_3^{(n)} r \sin \psi \\ -X_3^{(n)} r \cos \psi \\ 0 \\ 0 \end{Bmatrix} \tag{59}$$

and

$$X_3^{(n)} = \omega^2 m_s w + \int_0^{\bar{s}(1)} p_n(\bar{s},\bar{\xi})\ \bar{w}(\bar{\xi})\ \bar{R}(\bar{\xi})\ d\bar{\xi} \tag{60}$$

where m_s is the shell mass per unit of shell area and $p_n(\bar{s},\bar{\xi})$ is the nth trigonometric circumferential component of the pressure at some meridional location, $\bar{s}$, due to a unit of displaced liquid volume at meridional location, $\bar{\xi}$.

To evaluate $p_n(\bar{s},\bar{\xi})$, $\bar{w}(s)$ in equation (28) is set equal to a Dirac delta function which vanishes everywhere except at $\bar{s} = \bar{\xi}$, where it goes to infinity. Performing the integrations in equation (28) yield

$$\left[A - \eta\hat{A}_1 - \eta^2\hat{A}_2 - \eta^3\hat{A}_3\right]\{\bar{b}\} = \begin{Bmatrix} q_{1n}^*(\bar{\xi}) \\ q_{2n}^*(\bar{\xi}) \\ \cdot \\ \cdot \\ \cdot \\ q_{Mn}^*(\bar{\xi}) \end{Bmatrix} - \eta n_x \begin{Bmatrix} \frac{\partial}{\partial\bar{N}} q_{1n}^*(\bar{\xi}) \\ \frac{\partial}{\partial\bar{N}} q_{2n}^*(\bar{\xi}) \\ \cdot \\ \cdot \\ \cdot \\ \frac{\partial}{\partial\bar{N}} q_{Mn}^*(\bar{\xi}) \end{Bmatrix} \tag{61}$$

where

$$q_{mn}^*(\bar{\xi}) = q_{mn}(\bar{\xi}) - \eta\bar{\sigma}_m\, q_{m+M,n}(\bar{\xi}) \qquad (1 \leq m \leq M)$$

Solving for $\{\bar{b}\}$ in equation (61) and substituting into equation (24) result in

$$p_n(\bar{s},\bar{\xi}) = \rho_o\omega^2 \begin{Bmatrix} q^*_{1n}(\bar{s}) - \eta n_x \frac{\partial}{\partial \bar{N}} q^*_{1n}(\bar{s}) \\ q^*_{2n}(\bar{s}) - \eta n_x \frac{\partial}{\partial \bar{N}} q^*_{2n}(\bar{s}) \\ \vdots \\ q^*_{Mn}(\bar{s}) - \eta n_x \frac{\partial}{\partial \bar{N}} q^*_{Mn}(\bar{s}) \end{Bmatrix}^T \left[A - \eta\hat{A}_1 - \eta^2\hat{A}_2 - \eta^3\hat{A}_3\right]^{-1} \begin{Bmatrix} q^*_{1n}(\bar{\xi}) - \eta n_x \frac{\partial}{\partial \bar{N}} q^*_{1n}(\bar{\xi}) \\ q^*_{2n}(\bar{\xi}) - \eta n_x \frac{\partial}{\partial \bar{N}} q^*_{2n}(\bar{\xi}) \\ \vdots \\ q^*_{Mn}(\bar{\xi}) - \eta n_x \frac{\partial}{\partial \bar{N}} q^*_{Mn}(\bar{\xi}) \end{Bmatrix} \tag{62}$$

Since A, $\hat{A}_1$, $\hat{A}_2$, and $\hat{A}_3$ are symmetric matrices, it follows from linear algebra that $p_n(\bar{s},\bar{\xi})$ is symmetric, that is, $p_n(\bar{s},\bar{\xi}) = p_n(\bar{\xi},\bar{s})$. (See, for example, ref. 13.)

APPLICATIONS OF THEORY

The purpose of this section is to validate the pressure-series theory developed in this paper and to demonstrate its rate of convergence through appropriate examples. Two sets of examples are considered. The first deals with the sloshing of incompressible liquids in rigid cylindrical and hemispherical tanks. For the cylindrical tank, it is shown that the present theory yields the exact results; while for the hemispherical tank, correlation with other approximate theories provides validation. The second set of examples deals with the hydroelastic vibrations of incompressible liquids in a flexible propellant tank and in a flexible hemisphere. Validation is provided through correlation with NASTRAN analysis and experiment. For the hydroelastic results, the modified shell-of-revolution program discussed in the section entitled "Modified Shell Equations" was used.

Sloshing Motion of Incompressible Liquids in Rigid Tanks

General Considerations

From equation (46), the sloshing frequencies for incompressible liquids are given by the roots of

$$\text{Det}\left[A - \eta^*\hat{A}_1 - \eta^{*2}\hat{A}_2 - \eta^{*3}\hat{A}_3\right] = 0 \tag{63}$$

where the elements of A, $\hat{A}_1$, $\hat{A}_2$, and $\hat{A}_3$ depend on the values of λ_m. These values are arbitrary; however, judicious choices provide rapid convergence of the solution. An examination of some practical cases illustrates the manner in which λ_m may be selected.

Cylindrical Tanks

For cylindrical tanks, equation (63) greatly simplifies if λ_m ($m = 1,2,\ldots,M$) are the negative roots of

$$\frac{dJ_n}{d\zeta}(\zeta) = 0 \tag{64}$$

where $\zeta = \bar{R}\sqrt{-\bar{\lambda}_m}$. Then from equations (30) to (33) and (14) to (17), the integrals need only be carried out at $x = 1$ where $n_x = 1$ to give

$$A_{km} = \bar{\sigma}_m \int_0^{\bar{R}(1)} \left(q_{m+M,n} q_{kn}\right)_{\bar{x}=1} \bar{R}\, d\bar{r}$$

$$= \begin{cases} 0 & (k \neq m) \\ \bar{\sigma}_k\, \gamma_k^{(c)}(1)\, \gamma_k^{(s)}(1)\, \kappa_{kn} & (k = m) \end{cases} \tag{65}$$

$$\hat{A}_{1,km} = \begin{cases} 0 & (k \neq m) \\ \bar{\sigma}_k^2 \left[\gamma_k^{(s)}(1)\right]^2 \kappa_{kn} & (k = m) \end{cases} \tag{66}$$

$$\hat{A}_{2,km} = \begin{cases} 0 & (k \neq m) \\ \bar{\sigma}_k^2 \bar{c}_k\, \gamma_k^{(s)}(1)\, \gamma_k^{(c)}(1)\, \kappa_{kn} & (k = m) \end{cases} \tag{67}$$

$$\hat{A}_{3,km} = -\begin{cases} 0 & (k \neq m) \\ \bar{\sigma}_k^2 \bar{c}_k^2 \left[\gamma_k^{(s)}(1)\right]^2 \kappa_{kn} & (k = m) \end{cases} \tag{68}$$

where

$$\kappa_{kn} = \int_0^{\bar{R}(1)} z_{kn}^2(\bar{r})\, \bar{r}\, d\bar{r} \tag{69}$$

Substituting equations (65) to (68) into equation (63) gives

$$\left[\gamma_k^{(c)}(1) - \eta^* \bar{\sigma}_k\, \gamma_k^{(s)}(1)\right]\left[1 - \eta^{*2}\bar{\sigma}_k^2\right] = 0 \tag{70}$$

Hence, setting the first bracketed term of the left side to zero gives

$$\eta^* = \frac{1}{\bar{\sigma}_k} \coth \bar{\sigma}_k \tag{71}$$

which are the exact sloshing eigenvalues for cylindrical tanks. (See ref. 15, for example.) The roots of the second bracketed term are, from equation (47), associated with the vanishing of δp and are thus ignored.

Hemispherical Tanks

Since the selection of λ_m on the basis of equation (64) led to exact results for cylindrical tanks, it is reasonable to use this same selection basis for geometries of other tanks and allow the superposition of the series terms to satisfy the interface condition approximated by equation (13). To verify the validity of this approach, consider a hemispherical rigid tank of radius a and liquid height, h = a. Numerical solutions for M = 2, 9, and 10 are given in table I along with corresponding solutions from the literature as compiled in reference 6. It is seen that the series solution agrees reasonably well with published results and converges rapidly.

Hydroelastic Vibrations of Incompressible Liquids in Elastic Tanks

General Considerations

Previous investigations have concluded that gravity effects are almost always negligible in the hydroelastic vibration modes (ref. 1, ch. 9, and ref. 12, for example). Hence in this section, these effects are neglected (i.e., $\eta = 0$). From equation (62) the pressure loading on the shell is then

$$p_n(\bar{s},\bar{\xi}) = \rho_o \omega^2 \begin{Bmatrix} q_{1n} \\ q_{2n} \\ \cdot \\ \cdot \\ \cdot \\ q_{Mn} \end{Bmatrix}^T A^{-1} \begin{Bmatrix} q_{1n} \\ q_{2n} \\ \cdot \\ \cdot \\ \cdot \\ q_{Mn} \end{Bmatrix} \tag{72}$$

where the matrix A, as defined in equation (30), depends on q_{mn}, which in turn depends on the selected values of λ_m (see eqs. (14) to (17)). The

terms q_{mn} contain modified or unmodified Bessel functions depending on whether λ_m is positive or negative, respectively, and contain powers of r if $\lambda_m = 0$.

Following the line of reasoning in reference 7, one selects the positive set of λ_m as

$$\lambda_m = \left(\frac{m\pi}{h}\right)^2 \qquad (1 \leq m \leq M) \qquad (73)$$

and the negative set is selected to satisfy equation (64). Subsequently, the number of positive, negative, and zero values of λ_m selected are denoted by M_1, M_2, and M_3, respectively, whose sum is M.

Flexible Cylindrical Tanks

The motivation for using equations (64) and (73) to select λ_m is that these values lead to a pressure series which provides the exact solution for cylindrical tanks. (Compare pressure series with that of ref. 15.) In the next section, it is shown that even if the tank geometry is far from cylindrical, the superposition of these terms still yields accurate results when applied to the interface continuity condition of equation (13).

Flexible Propellant Tank and Comparison With Test

The propellant tank shown in figure 2 has been chosen for the purposes of this paper because it comprises a variety of geometries usually encountered in aerospace applications. The tank is composed of four distinct sections: a nearly spherical upper dome, a conical section, a cylindrical section, and a nearly ellipsoidal lower dome. A flange at the juncture of the lower dome and the cylindrical section of the tank is clamped to a heavy steel fixture shown in figure 2; thus a fully clamped condition was assumed in the analyses. The 1/8-scale tank approximates a liquid oxygen tank proposed for the space shuttle. Its specifications are given in appendix D.

Nonaxisymmetric and axisymmetric vibrations of the tank were investigated both analytically and experimentally. Both the present analysis and the NASTRAN hydroelastic analysis were used. The NASTRAN modeling is discussed in appendix C and the experimental procedure is discussed in appendix D.

Nonaxisymmetric modes.- Experimental and analytical results for the nonaxisymmetric modes of the propellant tank are compared in figures 3, 4, and 5. Natural frequencies are plotted as a function of the circumferential wave number n in figures 3(a), 4(a), and 5(a) for fill conditions of empty, three-quarters full, and full. Representative meridional mode shapes for a few select

values of n are illustrated in figure 3(b) for 1 and 2 half-waves along the shell meridian ($m = 1, 2$) and in figures 4(b) and 5(b) for 1, 2, and 3 half-waves along the shell meridian ($m = 1, 2, 3$).

Natural frequencies predicted by the present analysis are in excellent agreement with the experiment at all fill conditions and, in general, are somewhat more accurate than the NASTRAN results. Both the present analysis and the NASTRAN analysis included the effects of hydrostatic pressure induced on the shell wall from the weight of the liquid. The hydrostatic pressure produces a stiffening of the shell which increases with n. This effect is discussed more fully in a subsequent section of the paper.

For the empty tank, the curves of frequency versus the number of circumferential waves n for $m = 1$ and $m = 2$ cross at $n = 12$, whereas for an empty cylindrical tank, these curves, as would be expected, converge at higher values of n. The reason for this atypical behavior exhibited in figure 3(a) becomes apparent in figure 3(b). At $n = 2$, the lowest meridional mode is clearly $m = 1$ with nearly equal response on the cylindrical and conical sections of the tank. As n increases, however, the response of the cylindrical section decreases until at $n = 16$, virtually all of the response is in the conical section. Similarly, at $m = 2$, the response of the conical section decreases as n increases until at $n = 16$ all the response is in the cylindrical section. Thus at the higher circumferential wave numbers, the cylindrical and conical sections of the empty propellant tank behave essentially as separate entities.

The meridional mode shapes from the present analysis, which are virtually identical to those generated by NASTRAN, are shown in figures 3(b), 4(b), and 5(b). Qualitative experimental mode shapes were in agreement with the analytical results.

Axisymmetric modes.- Variation of the analytical and experimental frequencies for the first three axisymmetric ($n = 0$) vibration modes of the propellant tank are presented in figure 6(a) as a function of the liquid depth relative to the tank length (h/l). The agreement of both analyses with experiment is generally good. The undulating nature of the curves has been observed by others (ref. 16) and is thought to be a consequence of changes in the meridional mode shape.

The first three analytical meridional mode shapes are presented in figure 6(b), for several liquid depths. For clarity, only the mode shapes from the present analysis are shown. NASTRAN results are only slightly different except at the apex of the lower dome. As noted in appendix D, experimental axisymmetric nodal patterns could be detected only on the lower dome. These experimental lower dome nodal patterns are identified in figure 6(a) by the different test-point symbols and correlate well with the analytical lower dome mode shapes of figure 6(b).

Hydroelastic pressure effects in 1/8-scale tank.- As noted previously, the analytical results presented in figures 4(a), 5(a), and 6(a) include the effect of hydrostatic pressure. The magnitude of this effect on the nonaxisymmetric

shell frequencies of the propellant tank model may be observed in figure 7 by comparing the results of the present analysis including hydrostatic pressure (middle curve) with results from the same analysis without hydrostatic pressure (lower curve). Although the effect of hydrostatic pressure becomes substantial for $n > 6$, its effect is minimal at the lower values of n. If only the lower modes are of interest, as is often the case, the mathematical model may be simplified by neglecting the hydrostatic pressure with little loss of accuracy.

Hydrostatic pressure effects in equivalent full-scale tank.- Replica scaled models are commonly utilized to study the dynamic behavior of a structure in one of two ways. If the model includes sufficient structural detail, dynamic analysis may be foregone and full-scale behavior extrapolated from subscale test results. More commonly, dynamic tests of a simplified structural model are used to validate a mathematical model which in turn is applied to the full-scale structure. Caution must be exercised in using either approach to study the dynamic behavior of full-scale propellant tanks.

In general, the natural frequencies of a replica model are inversely proportional to the scale factor if the internal pressure of both model and full-scale counterpart are identical at corresponding locations. This requisite causes no difficulties in testing empty tanks but it would be necessary to test a 1/8-scale replica model containing liquid in a simulated 8g gravity field if the hydrostatic pressure of a full-scale tank at 1g is to be simulated.

Thus, substantial errors may result if hydrostatic pressure is neglected in applying the present analysis to an equivalent full-scale tank containing liquid. The magnitude of the effect of hydrostatic pressure for an equivalent full-scale tank filled with a liquid is shown by the difference between the upper and lower curves in figure 7. (Due to the scaling factor, all the frequencies indicated in this figure are 8 times those of a full-scale tank.) The upper curve results from the present analysis of the subject propellant tank (1/8-scale) in an 8g gravity field. As may be seen, the effect of hydrostatic pressure is much greater for the full-scale tank than for the 1/8-scale model. For $n = 6$, neglecting hydrostatic pressure effects results in a frequency prediction error of only 15 percent for the 1/8-scale model subjected to 1g but nearly 100 percent error for an equivalent full-scale tank at 1g. These scale effects of hydrostatic pressure would become even more pronounced if the longitudinal acceleration during flight was taken into account.

Free surface motion.- Figure 8 illustrates the free surface mode shapes for different numbers of circumferential waves n for $m = 1$, 2, and 3 meridional half-waves in the full and three-quarters full propellant tank. As indicated in figure 8, the entire free surface is moving when $n = 0$; however as n increases, the motion becomes localized to the shell wall with little motion occurring near the center line of the tank. This phenomenon is known to occur in practice and is readily accounted for in the present analysis by the modified Bessel functions in the series expansion. This helps to explain why the series expansion is so accurate for this type of problem.

It is also interesting to observe that the surface motion undergoes little change with meridional wave number. Consequently, mode shapes must be characterized by the motion of the shell wall.

Convergence of pressure series solution.- For the full propellant tank, analyses were performed using several combinations of M_1, M_2, and M_3 in order to study the significance of each type of series term in such problems.

The analyses were performed for the three lowest frequencies at $n = 6$, $m = 1$, 2, and 3; frequency results are presented as ratios to the corresponding converged values in table II. These results show that with $M_1 = 5$, converged frequencies are obtained irrespective of the values of M_2 and M_3. (As before, M_1, M_2, and M_3 are the number of user-selected positive, negative, and zero λ_m where the positive λ_m are given by equation (73) and the negative λ_m by equation (64).) Hence, only the positive set of λ_m need be selected, although addition of unnecessary terms did not deteriorate the results. Though not shown in table II, this conclusion has generally been true for all $n > 0$ (nonaxisymmetric modes); however, for $n = 0$ (axisymmetric modes), $\lambda_m = 0$ should be retained (i.e., $M_3 = 1$).

In figure 9, the series convergence at $n = 6$ is further examined for increasing values of M_1 with $M_2 = M_3 = 0$. It is clear from the figure that the convergence of the series is very rapid. Consequently, it is concluded that although the λ_m are selected on the basis of hydroelastic vibrations in cylindrical tanks, the same selection may be safely extended to other geometries.

Note that for nonaxisymmetric modes, the lower dome has negligible motion; hence the validity of the present analysis for such a dome undergoing nonaxisymmetric motion is not confirmed by the propellant tank results. To confirm the validity of the present analysis for such a dome, a partially filled elastic hemisphere is considered.

Flexible Hemisphere

The first two free edge modes of a partially water-filled aluminum hemisphere of radius a having two circumferential waves ($n = 2$) are shown in figure 10 for the full spectrum of fill conditions, $0 \leq h/a \leq 1$. Frequencies and mode shapes predicted using the present analysis are compared with NASTRAN results. For this comparison, the pressure loading on the shell wall, generated by NASTRAN, was applied to the structural program (refs. 8 to 10) used by the present analysis. Thus, any discrepancy between the two results can be attributed only to differences between the liquid finite-element analysis employed in NASTRAN and the pressure series analysis proposed herein. Since results for the propellant tank, previously discussed, indicated that only positive values of λ_m selected on the basis of equation (73) need be considered, only series terms corresponding to these values were used for the hemisphere. The convergence of the series expansion is indicated in figure 11. As in the case of the propellant tank, few terms need be retained.

In figure 10 the converged solutions of the present analysis for frequency and mode shape generally correlate very well with converged NASTRAN-generated solutions. This example further indicates that the use of a series containing products of modified Bessel functions and trigonometric functions ideally applicable to liquids in circular cylindrical tanks can be superimposed to

solve other geometries with adequate accuracy. Discrepancies between the two solutions in the second mode at low liquid height probably are due to the scarcity of liquid finite elements in the NASTRAN model near the bottom of the tank.

CONCLUDING REMARKS

An analysis is presented of hydroelastic vibrations of elastic tanks partially filled with incompressible nonviscous liquid in the presence of gravity. A complementary energy principle suitable for handling the liquid is derived, and the liquid is analyzed by using a series representation of the oscillatory pressure. By selecting each term of the series to satisfy the liquid governing equation (Laplace's equation), the energy principle reduces to an integral equation on the wetted portion of the tank wall. This integral equation represents an approximate statement of the liquid/elastic-tank compatibility at the wetted tank wall and may be solved numerically, without discretization of the liquid volume, to yield the pressure loading on the wall as a function of wall motion.

This approach permits the wall-motion-dependent liquid pressure loading to be readily incorporated into existing shell analysis computer programs. This procedure was followed to produce a modified shell-of-revolution program for hydroelastic vibrations. In the modified program presented herein, the pressure series terms (which must satisfy the governing liquid equation) were selected on the basis of a circular cylindrical tank geometry; that is, each term is a product of a modified (or unmodified) Bessel function and a trigonometric (or hyperbolic) function. The energy principle then allows solution of problems with geometries other than cylindrical by superposition of these terms. Application of the modified program to the gravity sloshing or hydroelastic vibrations of incompressible liquids in tanks of various geometries provides the following conclusions:

1. Since cylindrical functions are used as series terms, exact solutions are obtained for cylindrical tanks.

2. Sloshing frequencies for rigid hemispherical tanks correlated very well with published frequencies; and hydroelastic vibrations in an elastic propellant tank and in an elastic hemisphere also agreed well with test and finite-element (NASTRAN) results. Thus, the procedure can be applied to a wide variety of tank geometries.

3. Accurate results require retaining only a few terms in the series expansion.

4. Selection of the series terms is straightforward and is readily incorporated as an automatic feature of the modified program.

In addition, it is found that hydrostatic pressure from the liquid weight can cause significant stiffening of the tank wall and must therefore be accounted for, especially in full-scale fuel tanks on large space vehicles.

Langley Research Center
National Aeronautics and Space Administration
Hampton, VA 23665
October 30, 1979

APPENDIX A

LIQUID COMPLEMENTARY ENERGY PRINCIPLE

The purpose of this appendix is to formally state and confirm the validity of the liquid complementary variational principle used in the analysis presented in this paper. This principle is analogous to such principles in structures. The liquid pressures (or in structures, the stresses) are varied within a class of admissible pressures (or stresses); the admissible variations must satisfy Euler's equa ions (or the equations of motion) for perturbed motions about an initial state. When the variations are carried out, the complementary principle yields a compatibility equation (or equations) and boundary conditions on velocities (or displacements).

This appendix proceeds by first stating the principle, then establishing the admissible class of variations, deriving the appropriate variational complementary energies, and finally proving the principle.

Statement of Principle

Consider a nonviscous incompressible liquid which undergoes small irrotational harmonic oscillations, with the complex form $e^{j\omega t}$, about an initial pressurized state and in the presence of a gravitational field. The deformation state satisfies the compatibility relation,

$$\nabla^2\phi = 0 \tag{A1}$$

in V_o and

$$\frac{\partial\phi}{\partial N} = \dot{w} \tag{A2}$$

on S_w where $\dot{w}$ is applied. This deformation state makes the variation of the total complementary energy, Π_c, vanish, that is,

$$\delta\Pi_c = 0 \tag{A3}$$

provided that the variations satisfy Euler's equation and

$$\delta p = 0$$

on S_f. The next section of this appendix shows that constraining the variations to satisfy Euler's equation is equivalent to their satisfying a linearized form of Bernoulli's equation for small perturbations, namely,

$$\delta p = -\rho_o \delta\dot{\phi} + \rho_o g \delta u_x \tag{A4}$$

Furthermore,

$$\Pi_c = T_c - U_{c,g} - W_c \tag{A5}$$

where T_c, $U_{c,g}$, and W_c - the complementary kinetic, gravitational, and external work energies of the liquid, respectively - are derived in a subsequent section of this appendix.

Variation of Euler's Equation for Small Perturbed Motions

Euler's equation which expresses dynamic equilibrium for a nonviscous incompressible liquid is (see, for example, ref. 17, p. 95)

$$\rho_o \ddot{\tilde{U}} + \rho_o \left(\dot{\tilde{U}} \cdot \text{div}\right) \dot{\tilde{U}} + \text{grad } P - \rho_o g \text{ grad } x = 0 \tag{A6}$$

where the local Eulerian variables are as follows: ρ_o, the uniform mass density of the liquid; $\tilde{U}$, the velocity; and P the pressure. Considering a small perturbation about an initial pressurized state, one can write

$$\left.\begin{aligned} \dot{\tilde{U}} &= \dot{\tilde{u}} \\ P &= P_o + p \\ x &= x_o + u_x \end{aligned}\right\} \tag{A7}$$

In equations (A7), subscript o refers to the initial state and it is assumed that the liquid is initially at rest. Substituting equations (A7) into equation (A6) and neglecting nonlinear terms because the perturbations are assumed small yield

$$\rho_o \ddot{\tilde{u}} + \text{grad } p - \rho_o g \text{ grad } u_x + (\text{grad } P_o - \rho_o g \text{ grad } x_o) = 0 \tag{A8}$$

The term in parentheses vanishes since it represents equilibrium in the initial state and equation (A8) becomes

$$\rho_o \ddot{\tilde{u}} + \text{grad } p - \rho_o g \text{ grad } u_x = 0 \tag{A9}$$

APPENDIX A

By introducing the velocity gradient for irrotational flow, as given by equation (5) of the main text, into equation (A9),

$$\rho_o \text{ grad } \dot{\phi} + \text{grad } p - \rho_o g \text{ grad } u_x = 0$$

This equation may be integrated spatially to produce a linearized form of Bernoulli's equation for perturbed liquid motion, namely,

$$\rho_o \dot{\phi} + p - \rho_o g u_x = 0 \tag{A10}$$

where the constant of integration may be safely incorporated into ϕ as discussed in reference 1, page 15 and elsewhere. The variation of equation (A10) may now be taken to yield equation (A4).

Variational Complementary Forms of Kinetic, Gravitational, and External Energies

Complementary kinetic energy.- The well-known complementary kinetic energy is given as

$$T_c = \frac{1}{2} \int_{V_o} \rho_o \dot{\tilde{u}} \cdot \dot{\tilde{u}} \, dV_o \tag{A11}$$

where the integration may be safely carried out over the undeformed volume V_o since the liquid is assumed incompressible.

Substituting equation (5) into (A11) yields

$$T_c = \frac{1}{2} \int_{V_o} \rho_o \text{ grad } \phi \cdot \text{grad } \phi \, dV_o \tag{A12}$$

Taking the variation of both sides of equation (A12) results in

$$\delta T_c = \int_{V_o} \rho_o \text{ grad } \phi \cdot \text{grad } \delta\phi \, dV_o \tag{A13}$$

Green's theorem then provides

$$\delta T_c = -\int_{V_o} \rho_o \nabla^2\phi \, \delta\phi \, dV_o + \int_{S_o} \rho_o \, \text{grad} \, \phi \cdot \tilde{N} \, \delta\phi \, dS_o \tag{A14}$$

where $\tilde{N}$ represents an outward unit vector normal to the undeformed liquid surface S_o.

Complementary gravitational energy.- The variation of the complementary potential energy is found by considering the perturbed state of the liquid and varying the gravitational body forces which are given by

$$\tilde{F} = \rho_o g \, \text{grad} \, x$$

Taking the variation of $\tilde{F}$ and using equation (A7) gives

$$\delta\tilde{F} = \rho_o g \, \text{grad} \, (\delta u_x)$$

Hence the variation of complementary gravitational energy is

$$\delta U_{c,g} = \int_{V_o} \delta\tilde{F} \cdot \tilde{u} \, dV_o = \int_{V_o} \rho_o g \, \text{grad} \, \delta u_x \cdot \tilde{u} \, dV_o \tag{A15}$$

Substituting equation (5) into equation (A15) yields

$$\delta U_{c,g} = \frac{1}{j\omega} \int_{V_o} \rho_o g \, \text{grad} \, \delta u_x \cdot \text{grad} \, \phi \, dV_o \tag{A16}$$

Application of Green's theorem to equation (A16) gives

$$\delta U_{c,g} = -\frac{g\rho_o}{j\omega} \int_{V_o} \nabla^2\phi \, \delta u_x \, dV_o + \frac{g\rho_o}{j\omega} \int_{S_o} \frac{\partial\phi}{\partial N} \, \delta u_x \, dS_o \tag{A17}$$

APPENDIX A

Some previous authors (e.g., refs. 18 and 19) have used the Tong hypothesis, which states that

$$v_x \approx n_x(\tilde{u} \cdot \tilde{N}) = \frac{n_x}{j\omega} \frac{\partial \phi}{\partial N} \tag{A18}$$

where n_x is the cosine of the angle between the local surface normal $\tilde{N}$ and the x-axis. Under this hypothesis, the surface integral of equation (A17) becomes

$$\frac{g\rho_o}{j\omega} \int_{S_o} \frac{\partial \phi}{\partial N} \delta u_x \, dS_o \approx - \frac{g\rho_o}{\omega^2} \int_{S_o} n_x \frac{\partial \phi}{\partial N} \delta\left(\frac{\partial \phi}{\partial N}\right) dS_o \tag{A19}$$

Substituting equation (A19) into equation (A17) gives

$$\delta U_{c,g} = - \frac{g\rho_o}{j\omega} \int_{V_o} \nabla^2 \phi \, \delta u_x \, dV_o - \frac{g\rho_o}{\omega^2} \int_{S_o} n_x \frac{\partial \phi}{\partial N} \delta\left(\frac{\partial \phi}{\partial N}\right) dS_o \tag{A20}$$

Thus equation (A20) establishes the gravitational energy variation for a perturbing oscillation about an initial state of an incompressible liquid.

Complementary external work.- The variation of the complementary external work is

$$\delta W_c = - \int_{S_o} w \, \delta p \, dS_o \tag{A21}$$

where w is the perturbed displacement at the liquid surface in the $\tilde{N}$ direction. Substituting for δp from equation (A4), one has

$$\delta W_c = -\rho_o \int_{S_o} w(-j\omega \, \delta \phi + g \, \delta u_x) dS_o \tag{A22}$$

Use of the Tong hypothesis (eq. (A18)) yields

$$\delta W_c = j\omega\rho_o \int_{S_o} w \left[\delta \phi + \frac{g n_x}{\omega^2} \delta\left(\frac{\partial \phi}{\partial N}\right)\right] dS_o \tag{A23}$$

APPENDIX A

Proof of the Variational Principle (Eq. (A3))

Substituting equations (A14), (A20), and (A23) into equation (A3) results in

$$0 = \delta\Pi_c = \frac{1}{j\omega}\int_{V_o}\left[\rho_o\,\nabla^2\phi(-j\omega\,\delta\phi + g\,\delta u_x)\right]dV_o$$

$$+ \rho_o\int_{S_o}\left(\frac{\partial\phi}{\partial N} - j\omega w\right)\left[\delta\phi + \frac{gn_x}{\omega^2}\,\delta\left(\frac{\partial\phi}{\partial N}\right)\right]dS_o \qquad \text{(A24)}$$

Use of equation (A4) in the volume integrand of equation (A24) gives

$$0 = \delta\Pi_c = \frac{1}{j\omega}\int_{V_o}\nabla^2\phi\;\delta p\;dV_o + \rho_o\int_{S_o}\left(\frac{\partial\phi}{\partial N} - j\omega w\right)\left[\delta\phi + \frac{gn_x}{\omega^2}\,\delta\left(\frac{\partial\phi}{\partial N}\right)\right]dS_o \qquad \text{(A25)}$$

Since equation (A25) must be valid for all variations,

$$\nabla^2\phi = 0 \qquad \text{(A26)}$$

in V_o and

$$\frac{\partial\phi}{\partial N} = \dot{w}$$

on S_w and

$$\delta\phi + \frac{gn_x}{\omega^2}\,\delta\left(\frac{\partial\phi}{\partial N}\right) = 0 \qquad \text{(A27)}$$

on S_f which from equation (A4) is satisfied by the constraint $\delta p = 0$ on S_f. Hence, the principle is verified.

APPENDIX B

PROOF OF SYMMETRY OF MATRICES A, $\hat{A}_1$, $\hat{A}_2$, AND $\hat{A}_3$

To prove the symmetry of A as defined in equation (32), it suffices to show that

$$\int_{S_w} \left(\frac{\partial q_{mn}}{\partial \bar{N}} q_{kn} - \frac{\partial q_{kn}}{\partial \bar{N}} q_{mn} \right) dS_w = 0 \qquad (1 \leq m \leq M; \quad 1 \leq k \leq M) \qquad \text{(B1)}$$

Inasmuch as q_{mn} for $1 \leq m \leq M$ vanishes on the free surface ($x = 0$), the integration of equation (B1) may be carried out over the entire surface, S_o. Green's second formula then gives

$$\int_{V_o} \left(q_{kn} \nabla^2 q_{mn} - q_{mn} \nabla^2 q_{kn} \right) dV = 0 \qquad \text{(B2)}$$

But equation (B2) is valid as a consequence of equation (11); hence the proof is complete.

Similar proofs can be worked out for $\hat{A}_1$, $\hat{A}_2$, and $\hat{A}_3$.

APPENDIX C

NASTRAN MODELS OF PROPULSION TANK AND LIQUID

Finite-element frequencies and mode shapes used for comparison with results of the analysis presented in this paper were obtained using mathematical models described in this appendix. These models were developed within the NASTRAN hydroelastic capability (ref. 4) and modified according to references 2 and 3 to permit a symmetric fluid matrix formulation and thereby simplify computational procedures. The analysis is limited to incompressible fluids, and computational accuracy and efficiency are significantly increased by introducing a trigonometric series representation of circumferentially distributed displacements.

For the present purposes, the modified NASTRAN analysis was used only for the case of a free liquid surface, with gravity effects neglected. The analysis is valid also for the more general situation of a pressurized liquid level with gravity effects included.

Essentials of Modified NASTRAN Analysis for This Study

The theoretical development in reference 2 is based on the complementary energy principle applied to systems of discrete variables. The complementary kinetic energy of the liquid is the quadratic function

$$T_c = \frac{1}{2} \sum_i \sum_j L_{ij} \hat{p}_i \hat{p}_j \tag{C1}$$

written in terms of generalized impulsive pressures which are based on the pressure impulse definition

$$\hat{p} = \int_{-\infty}^{t} p \, dt \tag{C2a}$$

or

$$p = \dot{\hat{p}} \tag{C2b}$$

Since the liquid is assumed incompressible, there is no strain energy. The quantity L_{ij}, an element of the symmetric inverse mass matrix (termed inertance matrix in ref. 2), is defined as

$$L_{ij} = \frac{\partial^2 T_c}{\partial \hat{p}_i \, \partial \hat{p}_j} \tag{C3}$$

APPENDIX C

The complementary virtual work for the discretized system is expressed by

$$\delta W_c = \sum_k \sum_i A_{ik} \dot{u}_k^* \, \delta p_i \tag{C4}$$

where u_k^* is a discrete displacement of the liquid bounding surface and A_{ik} is the corresponding elemental generalized area as defined in reference 2.

Equations (C1) to (C4) are basic to the derivation of the Euler-Lagrange equations of motion of the liquid in reference 2. For the incompressible liquid, these equations are shown therein to reduce to the partitioned matrix equation,

$$\begin{bmatrix} L_{ff} & L_{fs} & L_{fi} \\ L_{sf} & L_{ss} & L_{si} \\ L_{if} & L_{is} & L_{ii} \end{bmatrix} \begin{Bmatrix} p_f \\ p_s \\ p_i \end{Bmatrix} = - \begin{bmatrix} A_{ff}^T & A_{sf}^T \\ A_{fs}^T & A_{ss}^T \\ 0 & 0 \end{bmatrix} \begin{Bmatrix} \ddot{u}_f \\ \ddot{u}_s \end{Bmatrix} \tag{C5}$$

where subscripts f, s, and i denote free liquid surface, liquid-structural interface (or wetted surface), and liquid interior, respectively. As a consequence of incompressibility, p_i may be related to $\left[p_f, p_s\right]^T$ so that

$$\begin{bmatrix} L'_{ff} & L'_{fs} \\ L'_{sf} & L'_{ss} \end{bmatrix} \begin{Bmatrix} p_f \\ p_s \end{Bmatrix} = \begin{bmatrix} A_{ff}^T & A_{sf}^T \\ A_{fs}^T & A_{ss}^T \end{bmatrix} \begin{Bmatrix} \ddot{u}_f \\ \ddot{u}_s \end{Bmatrix} \tag{C6}$$

in terms of the reduced inertance matrix

$$\begin{bmatrix} L'_{ff} & L'_{fs} \\ L'_{sf} & L'_{ss} \end{bmatrix} = \begin{bmatrix} L_{ff} & L_{fs} \\ L_{sf} & L_{ss} \end{bmatrix} - \begin{bmatrix} L_{fi} \\ L_{si} \end{bmatrix} \left[L_{ii}\right]^{-1} \begin{bmatrix} L_{ii} & L_{is} \end{bmatrix} \tag{C7}$$

For liquid displacements (or accelerations) normal to the free liquid surface, the off-diagonal area submatrices A_{fs}^T and A_{sf}^T vanish.

Dynamic coupling of the liquid with the tank structure is accomplished by introducing pressures determined from equation (C6) into a standard set of

structural dynamic equations, which may be written in the corresponding partitioned matrix form

$$\begin{bmatrix} 0 & 0 \\ 0 & M_s \end{bmatrix} \begin{Bmatrix} \ddot{u}_f \\ \ddot{u}_s \end{Bmatrix} + \begin{bmatrix} K_{ff} & K_{fs} \\ K_{sf} & K_{ss} \end{bmatrix} \begin{Bmatrix} u_f \\ u_s \end{Bmatrix} = \begin{bmatrix} A_{ff} & 0 \\ 0 & A_{ss} \end{bmatrix} \begin{Bmatrix} p_f \\ p_s \end{Bmatrix} \tag{C8}$$

Since the entire surface is constrained, that is,

$$\{p_f\} = 0 \tag{C9}$$

equation (C6) is solved to give

$$\{p_s\} = -\left[L'_{ss}\right]^{-1}\left[A^T_{ss}\right]\{\ddot{u}_s\} \tag{C10}$$

and

$$\{\ddot{u}_f\} = \left[A^T_{ff}\right]^{-1}\left[L'_{fs}\right]\left[L'_{ss}\right]\left[A^T_{ss}\right]\{\ddot{u}_s\} \tag{C11}$$

Substitution of equation (C10) into equation (C8) results in

$$\left[M_s + M_L\right]\{\ddot{u}_s\} + \left[K_{ss}\right]\{u_s\} = 0 \tag{C12}$$

which is the equation of free vibration of a liquid-loaded tank, with the liquid loading given by the liquid mass matrix

$$\left[M_L\right] = \left[A_{ss}\right]\left[L'_{ss}\right]^{-1}\left[A^T_{ss}\right] \tag{C13}$$

For simple harmonic motion, equation (C12) reduces to the familiar eigenvalue equation

$$\left[\left[K_{ss}\right] - \omega^2\left[M_s + M_L\right]\right]\{u\} = 0 \tag{C14}$$

which gives the frequencies and mode shapes of a liquid-loaded tank in free vibration.

APPENDIX C

Computer Program Implementation

The NASTRAN hydroelastic computer program of reference 4 is utilized and modified to implement the analysis of reference 2. As detailed in reference 3, the unsymmetric matrix formulation in the complex eigenvalue module (Rigid Format 7) is altered to compute the symmetric liquid mass matrix of equation (C13). The combination of this matrix with the tank structural mass and stiffness matrices, as indicated in equation (C14), is programmed in the normal vibration mode module (Rigid Format 3). The program modifications were made in accordance with the NASTRAN Direct Matrix Abstration Program (DMAP) for altering rigid formats.

Harmonic representations.- The liquid geometry is assumed to be axisymmetric, so that pressure distributions can be represented by a trigonometric series, such as (e.g., in ref. 2)

$$p(r_i,\theta_i,z_i) = p_o(r_i,z_i) + \sum_{k=1}^{n} \left[p_k(r_i,z_i) \cos k\theta_i + p_k^*(r_i,z_i) \sin k\theta_i \right] \qquad \text{(C15)}$$

in terms of circumferential harmonics ($n = 0,1,2,\ldots$), where p_k and p_k^* are generalized pressure amplitudes of symmetric and antisymmetric distributions, respectively. The condition of uniform pressure is given only for $n = 0$ in equation (C15). Harmonic pressure distributions such as equation (C15) are programmed in reference 4 and unchanged in reference 2.

A significant modification introduced in reference 2 is the trigonometric series representation of structural grid displacements consistent with equation (C15). Relationships between discrete-displacement and harmonic-displacement amplitudes are listed therein for cylindrical and spherical coordinate systems. All rigid-body motions are included in these relations. The transformations from discrete to harmonic displacements (in ref. 2) are made by including multipoint constraints (MPC) of the form

$$\{u_g\} = [G_{gh}]\{u_h\} \qquad \text{(C16)}$$

in the input data, where $\{u_g\}$ is the discrete grid displacement vector, $\{u_h\}$ is the harmonic-displacement vector, and $[G_{gh}]$ is the MPC transformation matrix. Elements of $[G_{gh}]$ are trigonometric functions evaluated at discrete-variable grid locations of the tank structure. Harmonic displacements are oriented to a set of fictitious grid points distributed along the tank meridian and distinct from physical grid points. At each meridian in the physical grid system, physical grid points around the circumference are related to the so-called harmonic grid points by equation (C16).

This transformation not only makes displacement and pressure representations consistent but can also result in large reductions in the number of degrees of freedom for hydroelastic dynamic analysis. For all six degrees of freedom at each physical grid point, the maximum number of degrees of freedom in

the physical system is $6 \times J \times K$, where J denotes the number of meridians and K the number of circumferential grid points at each meridian. This triple product is the dimension of $\{u_g\}$ (i.e., number of rows) in equation (C16). If N denotes the number of harmonics (or circumferential wave numbers $n = 0,1,2,\ldots$) included in the analysis, the dimension of $\{u_h\}$ is $6 \times N$, and since N is usually much smaller than either J or K, equation (C16) can result in a radical reduction in problem size, namely N/JK. Still further reduction is possible by omitting generalized rotation and tangential degrees of freedom in a Guyan reduction, with harmonic grid points referenced in NASTRAN OMIT instructions.

Computations of liquid pressures and masses.- Liquid finite elements in NASTRAN are rectangular and triangular solids of revolution interconnected by concentric rings comprising the liquid grid system. The liquid elements (CFLUIDi, i=2,3,4) and their ring boundaries (RINGFL specifications) are analogous to structural finite elements and grid points, respectively. Liquid incompressibility is represented by removal of internal pressure degrees of freedom $\left(\{p_i\}\right.$ in eq. (C5)$\left.\right)$ by means of a special OMIT instruction in which the concentric rings are referenced by a 7-digit integer numbering system. The surface pressure constraints in equation (C9) are represented by special single-point constraints (SPC), also referencing the 7-digit ring identification. The wetted tank surface is represented by GRIDB instructions which relate structural grid points (GRID) there with liquid-element boundaries. Since liquid pressures calculated by equation (C10) depend primarily on outward normal (or radial) accelerations, rotations and tangential displacements are constrained (by SPC instructions), and MPC relations between physical and harmonic degrees of freedom (eq. (C16)) are reduced by a factor of 6.

The symmetric fluid mass matrix given by equation (C13) is calculated by modifying the program steps of Rigid Format 7 so that the complex eigenvalue routine (CEAD) is not used. These modifications are specified in reference 3 by DMAP ALTER instructions for matrix printout, partitioning, and matrix inversion to form the liquid inertance, surface area, free surface accelerations (or displacements), pressure, and mass matrices of equations (C10), (C11), and (C13). Along with these types of instructions are direct matrix input (DMI) specifications in the input data in the form of partitioning vectors to identify pressure and displacement degrees of freedom. The OUTPUT3 DMAP instruction causes the liquid pressure and mass matrices to be punched on cards in DMI format.

Vibration modes of liquid-loaded tank.- Liquid pressures and masses, plus free surface motions (eq. (C11)), as desired, output in Rigid Format 7 are input as data in Rigid Format 3 to obtain normal free vibration modes. Liquid-structural coupling is directed by DMAP ALTER instructions as shown in reference 3 prior to execution of the real eigenvalue routine (READ). The tank structure is modeled by flat plate elements (CQUAD2) interconnected by grid points. Harmonic grid points are included, as in the liquid model, and the MPC relations include harmonic representations of all six degrees of freedom (three displacements and three rotations) at each physical grid point. Rotations and tangential displacements, constrained by SPC instructions in Rigid Format 7, are removed by OMIT instructions in Rigid Format 3.

APPENDIX C

NASTRAN Models

NASTRAN finite-element models of the liquid-loaded elastic propellant tank of figure 2 are illustrated in figures 12 and 13. The model in figure 12 is similar to that used in references 2 and 3 except for the liquid element boundaries in figure 12(a). A finer grid model is shown in figure 13. Free surface motions, given by equation (C11), were not sought. Physical and harmonic grid points in the upper and lower domes and in the conical section are oriented in spherical coordinates, and grids in the cylindrical section are in cylindrical coordinates. The closer spacing between concentric rings near the tank wall is intended to simulate more accurately large pressure gradients there, particularly for higher circumferential wave numbers (or harmonics). The meridional liquid grid locations match the meridional structural grid locations along the wetted surface.

Liquid models.- The coarse liquid grid system in figure 12(a) consists of 15 meridional stations with 4 liquid-element boundaries at each meridian except 3 near the tank bottom which have fewer boundaries. The model has a total of 1386 possible pressure and displacement degrees of freedom. The free surface pressures are constrained by 16 liquid SPC statements, and all but the radial displacements are constrained by 987 structural SPC's. Incompressibility accounts for another 132 pressure degrees of freedom being removed by liquid OMIT statements. Harmonic representations of radial displacements through MPC relations account for another 135 degrees of freedom.

There are 116 degrees of freedom remaining, of which 56 are pressures and 60 are displacements. Four harmonics (N = 4) are included in this mode, n = 0 to 3, so that (J-1)N = 56 and JN = 60, where J in this case is 15. These integer products determine the matrix sizes and partitions for liquid pressures and masses on the DMI specifications for the vector P9 in the DMAP ALTERS of reference 3. The pressure matrix (PDU2) in reference 3 computed for this model is rectangular with 56 rows and 60 columns, and the symmetric liquid mass matrix (MFLD) is 60 × 60.

The fine liquid grid system in figure 13(a) consists of 28 meridional stations with 6 liquid-element boundaries at each meridian except 2 meridians closest to the tank bottom, where 4 and 5 rings bound 5 liquid elements. The maximum number of degrees of freedom for this model is 3537. There are 2818 SPC statements, of which 6 are fluid SPC's constraining free surface pressures. Liquid OMIT statements account for 132 degrees of freedom and MPC relations for another 532. In the remaining 55 degrees of freedom, there are 27 pressures and 28 displacements. With one harmonic at a time (N = 1) in this model, the number of displacements is the same as the number of meridians (J = 28, N = 1), and the number of pressures is one less. Thus, the liquid pressure matrix is 27 × 28 and the liquid mass matrix 28 × 28.

For partially filled tanks, the number of pressures is reduced, but not the number of displacements. The reduced number of pressures is obtained by subtracting more than one meridian from J for the full tank; that is, J-1 becomes J-2, J-3, J-5, and so forth for various reduced levels of the liquid. Pressures above the liquid surface are constrained by liquid SPC statements.

APPENDIX C

Structural models.- The coarse structural model of figure 12(b) has 9 physical grid points around half the circumference at each meridian, with a 22.5° interval between circumferential grid points. The top and bottom domes are modeled by triangular plate elements (CTRIA2) which connect the apex grid points to the grid points at the full tank level and at the lowest meridian. The maximum number of degrees of freedom is 1182, including 60 harmonic displacements. Constraints (SPC) are applied to 72 degrees of freedom, of which 48 satisfy boundary conditions for motions associated with $n = 0$ that are symmetric with respect to the pitch plane of symmetry. The remaining 24 constrained degrees of freedom simulate the tank mounting in the test program (appendix D), that is, the clamped ring modeled by beam elements (CBAR), at the base of the cylindrical section. Application of the Guyan reduction accounts for 240 omitted degrees of freedom (on OMIT statements), of which 28 are associated with harmonic $n = 0$ and the rest with harmonics $n = 1$, 2, and 3. There are 810 MPC relations to implement the harmonic representation of all 6 physical degrees of freedom at each grid point. The remaining degrees of freedom number 60. Although harmonics $n = 1$, 2, and 3 are included in the calculations, vibration modes of tank and fluid are reported only for variations in tank fullness associated with the axisymmetric mode $n = 0$, for which the coarse liquid and structural grids illustrated in figure 12 are considered adequate.

The fine structural model of figure 13(b) has 19 physical grid points around a quarter of the circumference at each of 30 meridians, with a 5° interval between circumferential grid points. Two of these meridians lie above the full tank level, and apex grid points are connected to the highest and lowest meridians by triangular plate elements. There are a total of 3612 physical and harmonic degrees of freedom which reduce to 28 harmonic degrees of freedom. Constraints specifying symmetric boundary conditions at the apexes plus clamped ring constraints total 12. The Guyan reduction is applied to the apexes, consistent with symmetric boundary conditions, for all harmonic degrees of freedom at the two meridians above the full tank level and for all but the harmonic radial degree of freedom over the wetted tank surface. The number of omitted degrees of freedom totals 152. Harmonic representation accounts for 3420 degrees of freedom. The fine model was used to calculate liquid-loaded vibration modes for nonaxisymmetric modes ranging from $n = 2$ to 16 for both three-quarters full and full tanks.

Hydrostatic pressure loading.- The effect of hydrostatic pressure was introduced into the NASTRAN finite-element model by determining an additional stiffness matrix $[\Delta K]$ equivalent to the matrix product $-[T]^{-1}[\Gamma]$ in equation (56). Static pressures at a given fluid depth were calculated by the product of the depth by the unit weight of liquid and were uniformly distributed over quadrilateral plate elements forming the tank boundary at that depth. These pressure loads were computed for every row of plate elements from the liquid level to the tank bottom and were input (on PLOAD2 statements) to the structural model for $n = 0$. This model was then run in the NASTRAN differential stiffness module (Rigid Format 4) which was instructed by DMAP ALTER to output $[\Delta K]$ onto magnetic tape. This additional stiffness matrix was then read (also by DMAP ALTER) into Rigid Format 3 and added to the structural

stiffness matrix $\left[K_{ss}\right]$. The eigenvalue equation (C14) was then solved in the usual manner to obtain the natural frequencies and mode shapes of the liquid-loaded tank under hydrostatic pressure. The effect of this hydrostatic pressure loading was determined for full and three-quarters full tanks for nonaxisymmetric modes using the fine-grid model of figure 13.

APPENDIX D

PROPELLANT TANK TESTS

This appendix contains a brief description of the propellant tank referred to in the main text and the equipment and procedure used to obtain the data presented therein.

Propellant Tank

The propellant tank depicted in figure 2 is a 1/8-scale model of an early version of the space shuttle liquid-oxygen tank. The tank is made up of four aluminum sections: an upper dome of nearly spherical shape, a conical section, a cylindrical section, and a lower dome of nearly ellipsoidal shape. The overall diameter and height of the tank are approximately 1 and 2 meters, respectively. The wall thicknesses of the various sections are indicated in figure 2. A flange at the juncture of the lower dome and cylindrical section of the tank is clamped to a heavy steel test fixture shown in figure 2.

Nonaxisymmetric Tests ($n \neq 0$)

Sinusoidal excitation of the tank was provided by a small servocontrolled electrodynamic exciter driving normal to the surface of the cylindrical or conical section of the tank and, where applicable, below the liquid surface. Maximum force capability of the exciter was 4.4 newtons. A force gage used to monitor the input force was installed between the exciter and tank shell. A servocontrol and oscillator were employed to maintain a constant sinusoidal exciter force.

The response of the shell was detected by a motorized noncontacting displacement transducer which traversed a circular track (fig. 2). The track could be positioned at any desired station along the length of the tank. A coincident-quadrature analyzer was used to measure the quadrature component of the displacement (90° out of phase with the input force). Resonance was determined by manually adjusting the exciter frequency at a given level of input force until a maximum quadrature component was obtained. The circumferential mode shape was then recorded by inputting the quadrature component of the displacement into an x-y plotter as the transducer traversed the circumference of the tank. Qualitative longitudinal variation of the mode shapes was obtained by observing the Lissajous pattern on an oscilloscope screen as a hand-held velocity transducer was moved to several axial stations along the tank. Vibration modes were measured for liquid (water) depths of 0, 1.27, and 1.90 meters corresponding nominally to empty, three-quarters full, and full conditions.

Axisymmetric Tests ($n = 0$)

For the axisymmetric vibration modes, analyses indicate (fig. 6(b)) that the largest vibration amplitudes occur below the liquid level and that at the

greater liquid depths, the vibration amplitude of the conical and cylindrical sections are of magnitude comparable with that on the lower dome. In the laboratory, however, the response of the cylindrical and conical tank sections in the high-energy axisymmetric modes is completely masked by the large response in the neighboring low-energy nonaxisymmetric modes. The problem is further aggravated for this particular tank by the high modal density of the nonaxisymmetric shell modes in the same frequency range as the axisymmetric modes. Axisymmetric nodal patterns were identifiable, however, on the lower dome, and in figure 6(a) the resonant frequencies of the first three lower-dome $n = 0$ modes are plotted as a function of the liquid depth. Except at the shallower liquid depths, an axisymmetric dome response was always coupled to a much larger nonaxisymmetric response of the cylindrical and conical sections; thus, most of the data points of figure 6(a) are in reality the resonant frequencies of $n \neq 0$ shell modes in proximity to the resonant frequencies of the $n = 0$ dome modes. In some cases, two or more $n = 0$ dome responses having the same nodal pattern were present in a small frequency band. If the response at one frequency was appreciably larger than the others, only one data point was recorded. If the response of two closely spaced resonances were of comparable magnitude, both frequencies were recorded.

Many of the axisymmetric modes did not exhibit classical characteristics in that where one segment of the lower dome contained only one circumferential node, another segment might contain two. Such cases are designated in figure 6(a) by the superposition of the appropriate nodal pattern symbols.

The noncontacting probe and track assembly used for the nonaxisymmetric shell modes could not be readily adapted to measure responses on the lower dome. The modal patterns on the lower dome were detected either by touch or through the use of a movable vacuum-attached accelerometer and Lissajous patterns.

REFERENCES

1. Abramson, H. Norman, ed.: The Dynamic Behavior of Liquids in Moving Containers. NASA SP-106, 1966.

2. Coppolino, R. N.: A Numerically Efficient Finite Element Hydroelastic Analysis. NASA CR-2662, 1976.

3. Coppolino, Robert N.: A Numerically Efficient Finite Element Hydroelastic Analysis. Volume II: Implementation in NASTRAN - Parts I and II. NASA CR-132684, 1974.

4. McCormick, Caleb W., ed.: The NASTRAN User's Manual (Level 15.0). NASA SP 222(01), 1973.

5. SPAR Structural Analysis System Reference Manual - System Level 11. NASA CR-145098, 1977.

6. Khabbaz, Ghassan R.: Dynamic Behavior of Liquids in Elastic Tanks. LMSC 60-80-70-23, Lockheed Missiles & Space Co., Aug. 1970.

7. Housner, Jerrold M.; and Herr, Robert W.: Vibrations of Incompressible Liquid-Elastic Tank Combinations Using a Series Representation of the Liquid. Computational Methods for Fluid-Structure Interaction Problems, T. Belytschko and T. L. Geers, eds., AMD - Vol. 26, American Soc. Mech. Eng., Nov.-Dec. 1977, pp. 49-64.

8. Cohen, Gerald A.: Computer Analysis of Asymmetric Free Vibrations of Ring-Stiffened Orthotropic Shells of Revolution. AIAA J., vol. 3, no. 12, Dec. 1965, pp. 2305-2312.

9. Cohen, Gerald A.: Computer Analysis of Ring-Stiffened Shells of Revolution. NASA CR-2085, 1973.

10. Cohen, Gerald A.: User Document for Computer Programs for Ring-Stiffened Shells of Revolution. NASA CR-2086, 1973.

11. Hwang, Chintsun: Longitudinal Sloshing of Liquid in a Flexible Hemispherical Tank. Trans. ASME, Ser. E: J. Appl. Mech., vol. 32, no. 3, Sept. 1965, pp. 665-670.

12. Pinson, Larry D.; and Brown, Christine G.: A Finite Element Method for Nonaxisymmetric Vibrations of Pressurized Shells of Revolution Partially Filled With Liquid. AIAA Paper 73-399, Mar. 1973.

13. Rabenstein, Albert L.: Elementary Differential Equations With Linear Algebra. Academic Press, c.1970.

14. Chu, Wen-Hwa: Breathing Vibrations of a Partially Filled Cylindrical Tank - Linear Theory. Trans. ASME, Ser. E: J. Appl. Mech., vol. 30, no. 4, Dec. 1963, pp. 532-536.

15. Mixson, John S.; and Herr, Robert W.: An Investigation of the Vibration Characteristics of Pressurized Thin-Walled Circular Cylinders Partly Filled With Liquid. NASA TR-145, 1962.

16. Coale, C. W.: Axisymmetric Vibrations of a Cylindrical-Hemispherical Tank Partially Filled With a Liquid. AIAA J., vol. 7, no. 2, Feb. 1969, pp. 235-243.

17. Shames, Irving H.: Mechanics of Fluids. McGraw-Hill Book Co., Inc., 1962.

18. Tong, Pin: Liquid Sloshing in an Elastic Container. AFOSR66-0943, U.S. Air Force, June 1966. (Available from DDC as AD 637 233.)

19. Anquez, Louis; Burger, Henri; Ohayon, Roger; and Valid, Roger: Vibrations of Tanks Partially Filled Witn Liquids. ONERA T.P. 1323, Jan. 1974.

TABLE I.- SLOSHING FREQUENCIES IN A RIGID HEMISPHERICAL TANK

n	Frequency parameter, $1/\eta = \omega^2 h/g$					
	Results compiled in ref. 6			Present solution ($M_1 = M_3 = 0$)		
	Finite elements	Method of ref. 6	Integral solution	$M_2 = 2$	$M_2 = 9$	$M_2 = 10$
0	3.96	3.92	3.65	3.862	3.791	3.790
1	1.57	1.68	1.56	1.620	1.594	1.592
2	----	3.03	----	2.925	2.889	2.887
3	----	4.34	----	4.295	4.349	4.359
4	----	5.62	----	5.370	5.411	5.414
5	----	6.88	----	6.445	6.473	6.475

TABLE II.- EFFECTS OF THE THREE TYPES OF SERIES TERMS

ON THE $n = 6$ PROPELLANT TANK FREQUENCIES

[Subscript c refers to converged results and subscripts 1, 2, and 3 refer to m = 1, 2, and 3.]

M_1	M_2	M_3	$M = \sum_{i=1}^{3} M_i$	ω_1/ω_{1c}	ω_2/ω_{2c}	ω_3/ω_{3c}
5	0	0	5	1.00	1.01	1.09
0	1	0	1	7.04	7.37	6.47
0	5	0	5	7.06	6.39	5.93
0	0	1	1	1.74	5.12	6.45
5	5	1	11	1.00	1.01	1.09

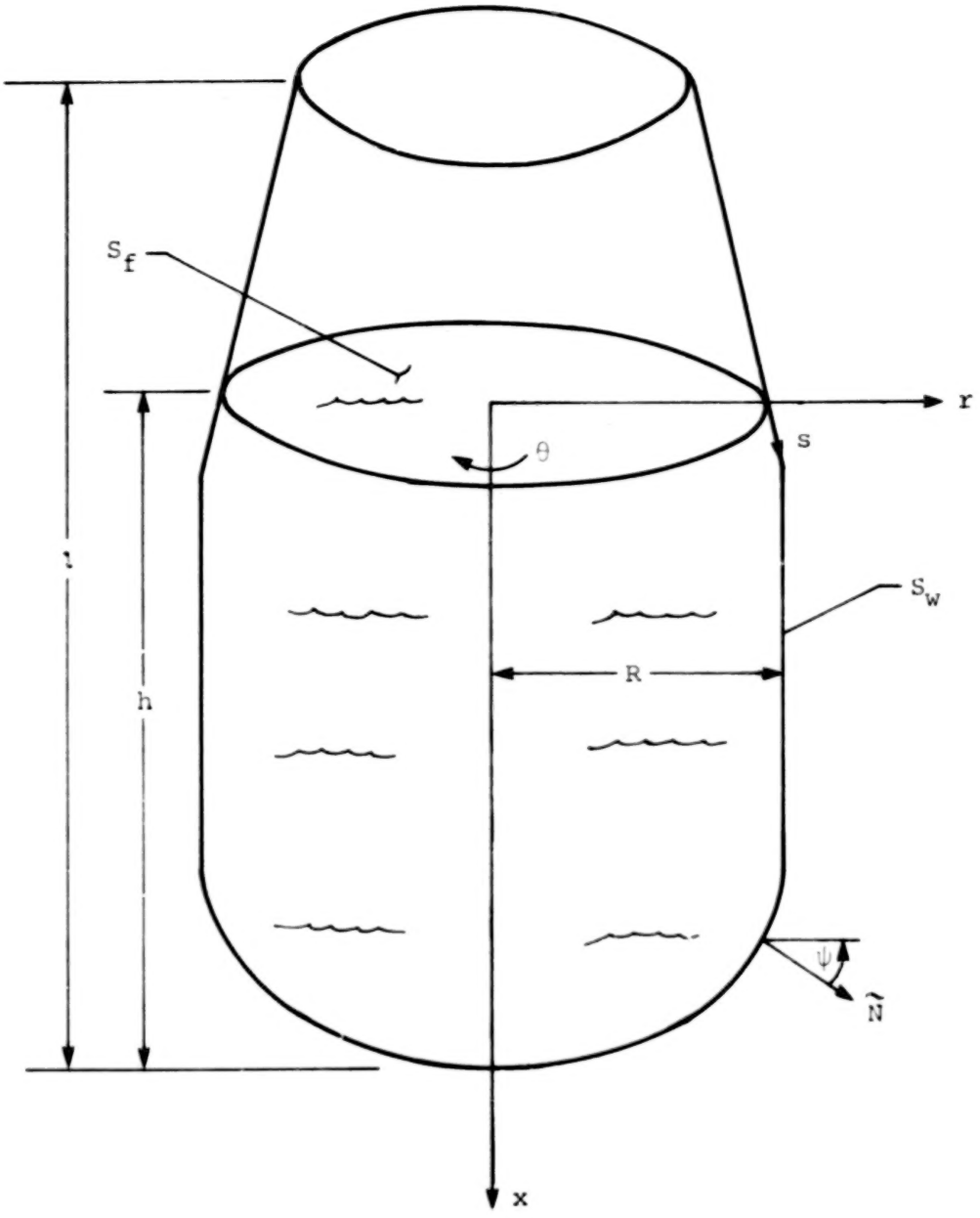

Figure 1.- General tank geometry and coordinates.

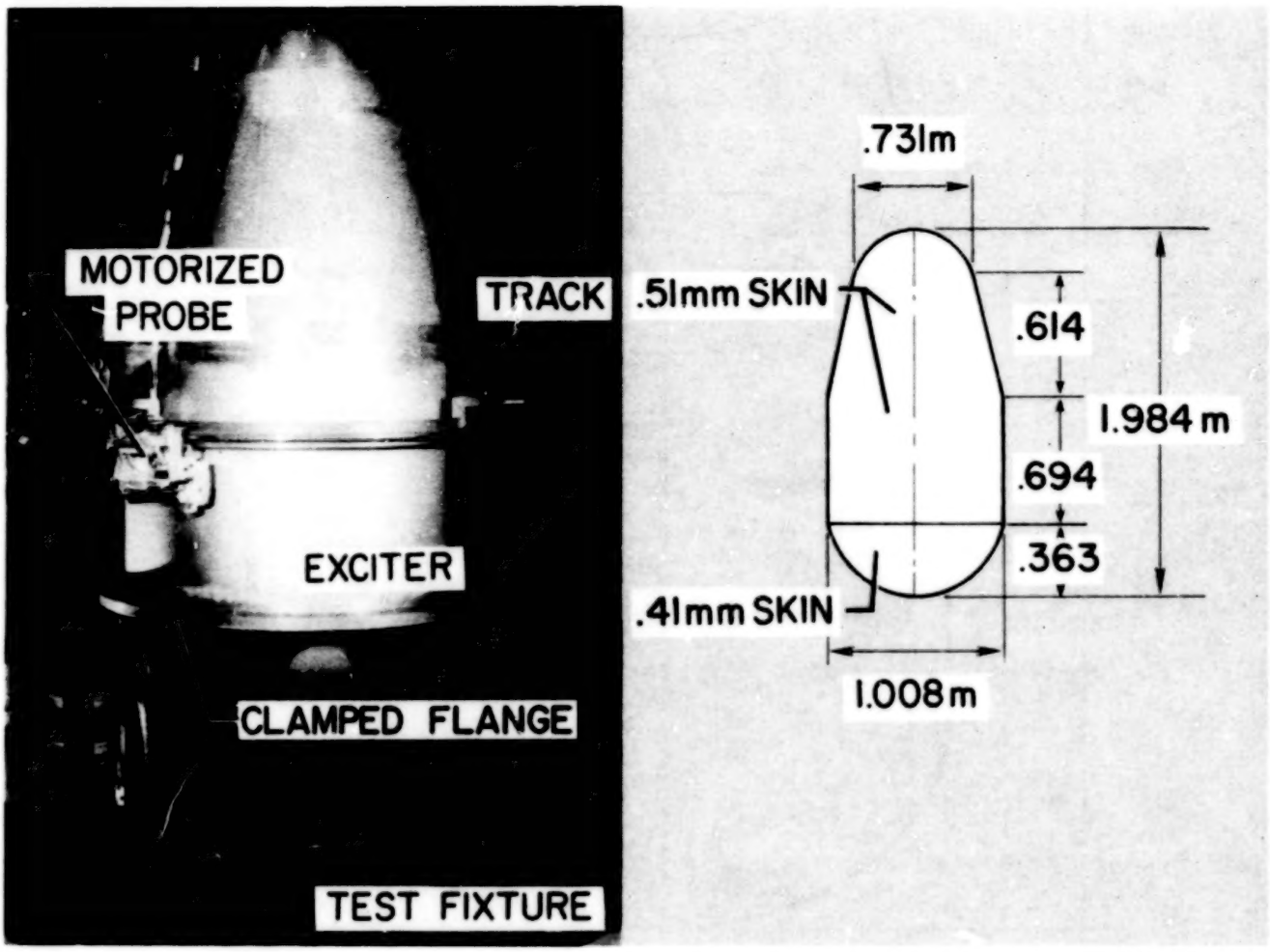

L-79-314

Figure 2.- Experimental apparatus and dimensions of propellant tank.

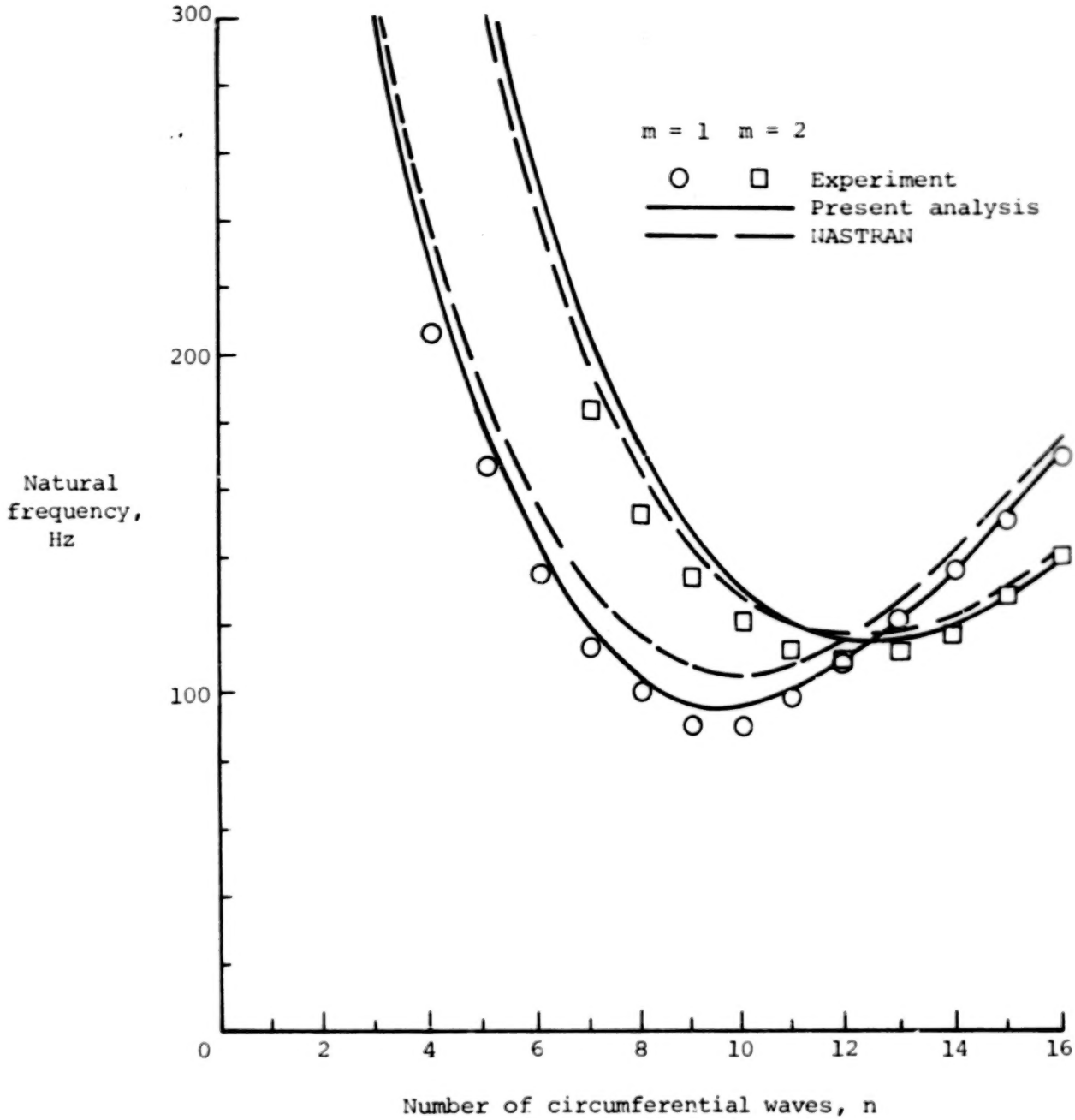

(a) Natural frequency.

Figure 3.- Nonaxisymmetric vibration modes of empty propellant tank.

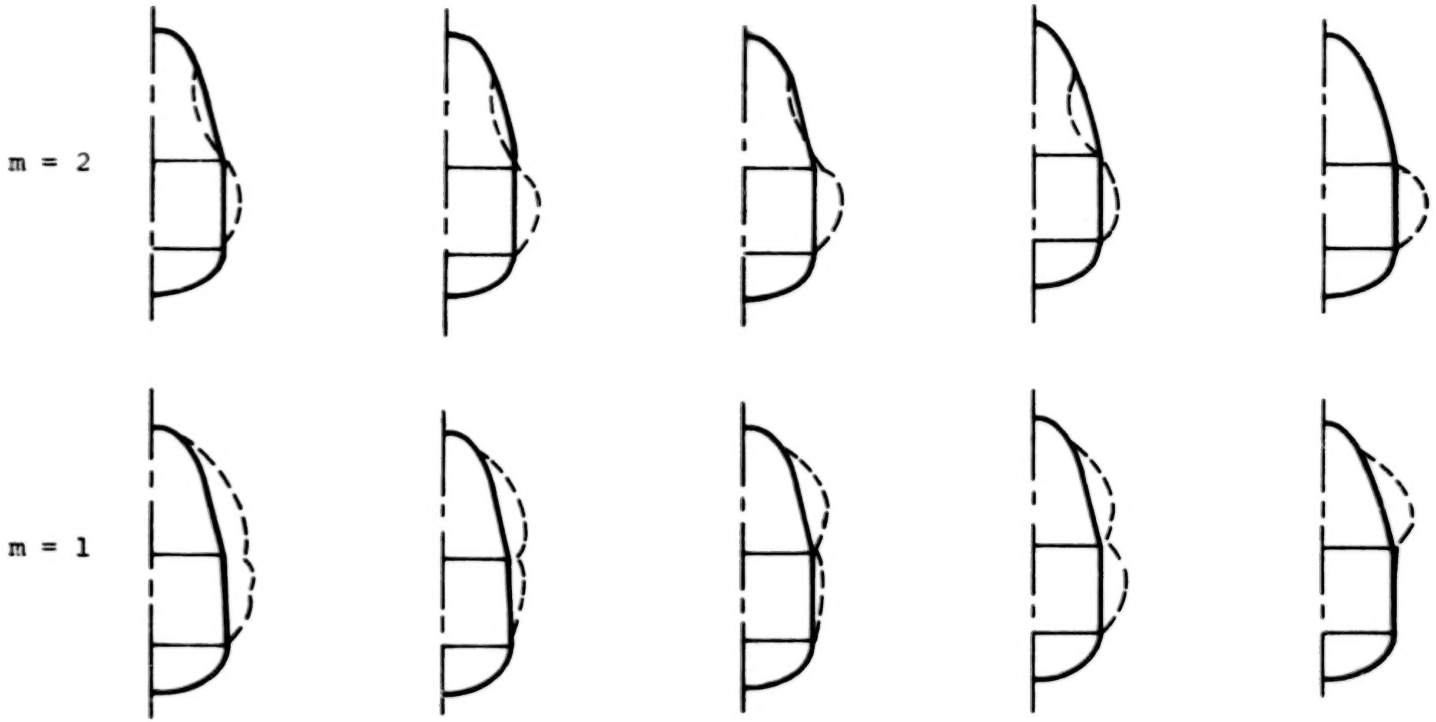

(b) Analytical meridional mode shapes.

Figure 3.- Concluded.

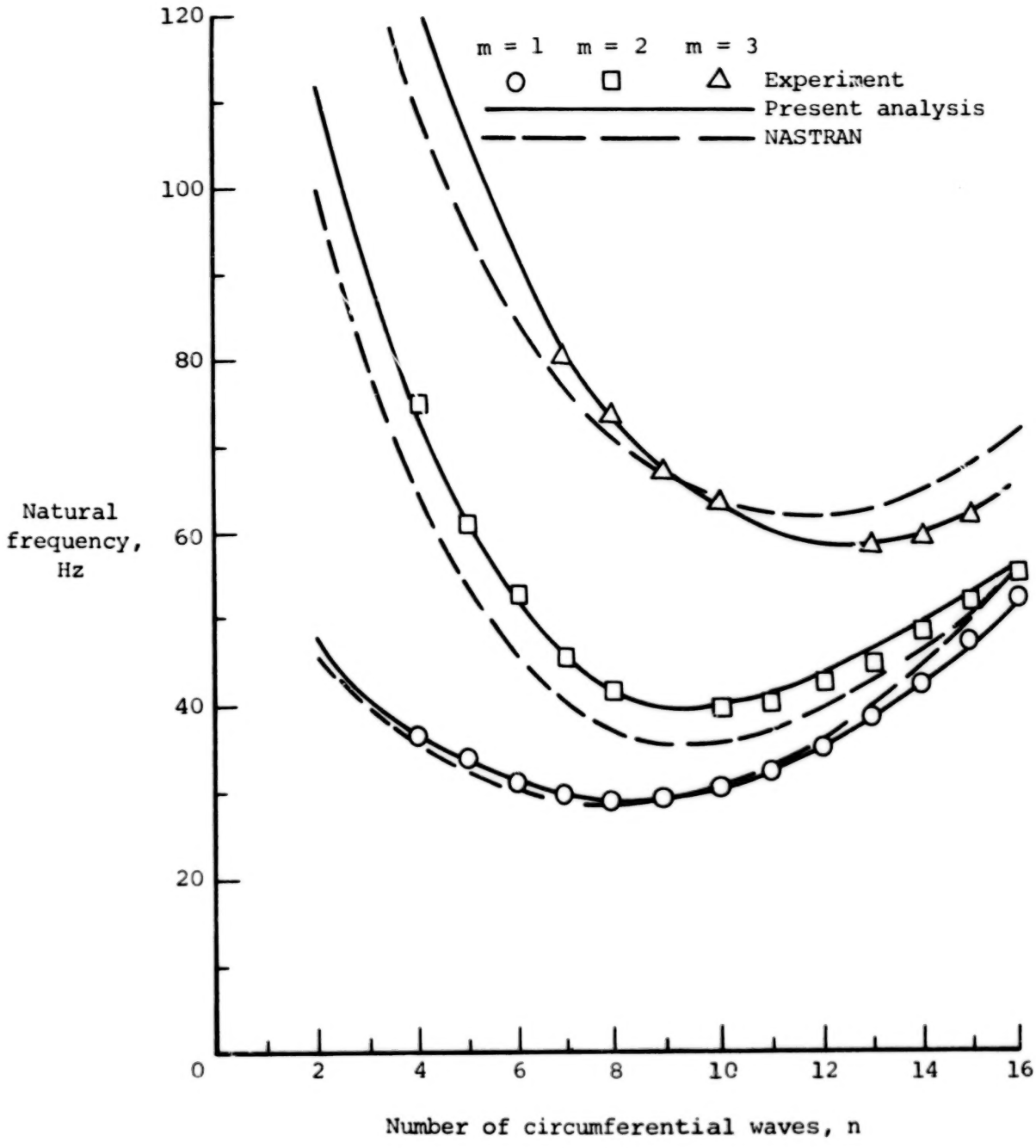

(a) Natural frequency.

Figure 4.- Nonaxisymmetric vibration modes of three-quarters full propellant tank.

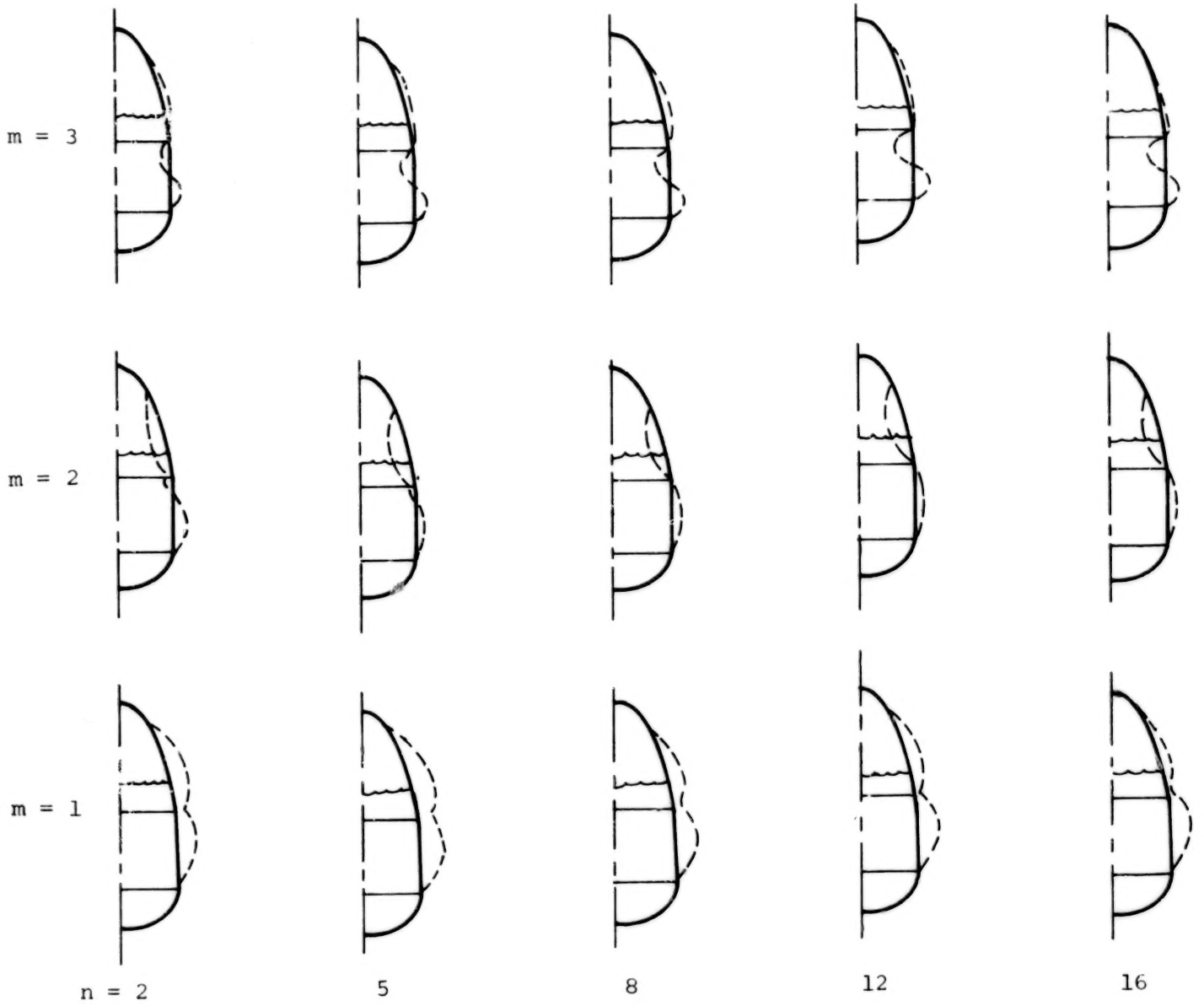

(b) Analytical meridional mode shapes.

Figure 4.- Concluded.

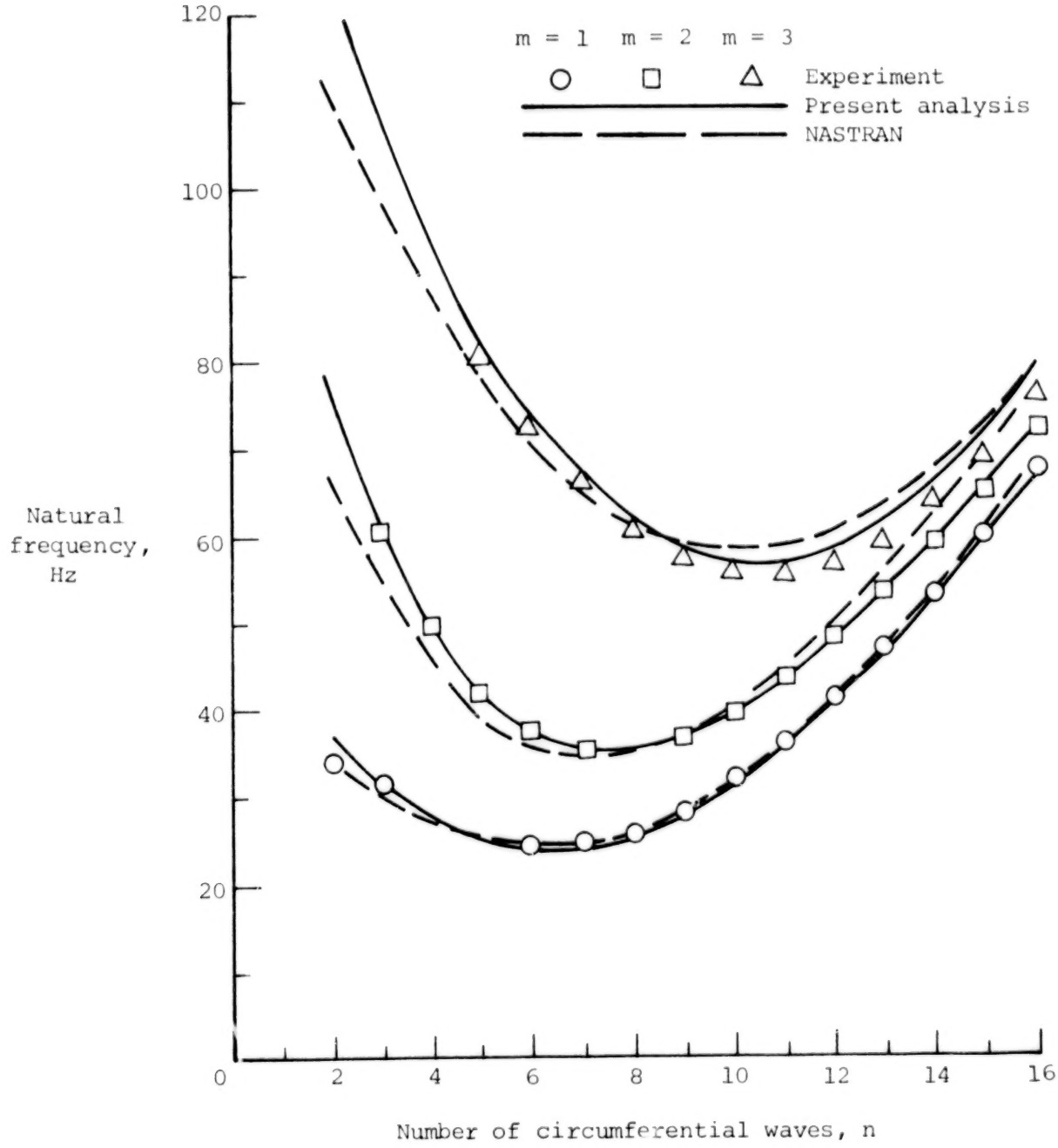

(a) Natural frequency.

Figure 5.- Nonaxisymmetric vibration modes of full propellant tank.

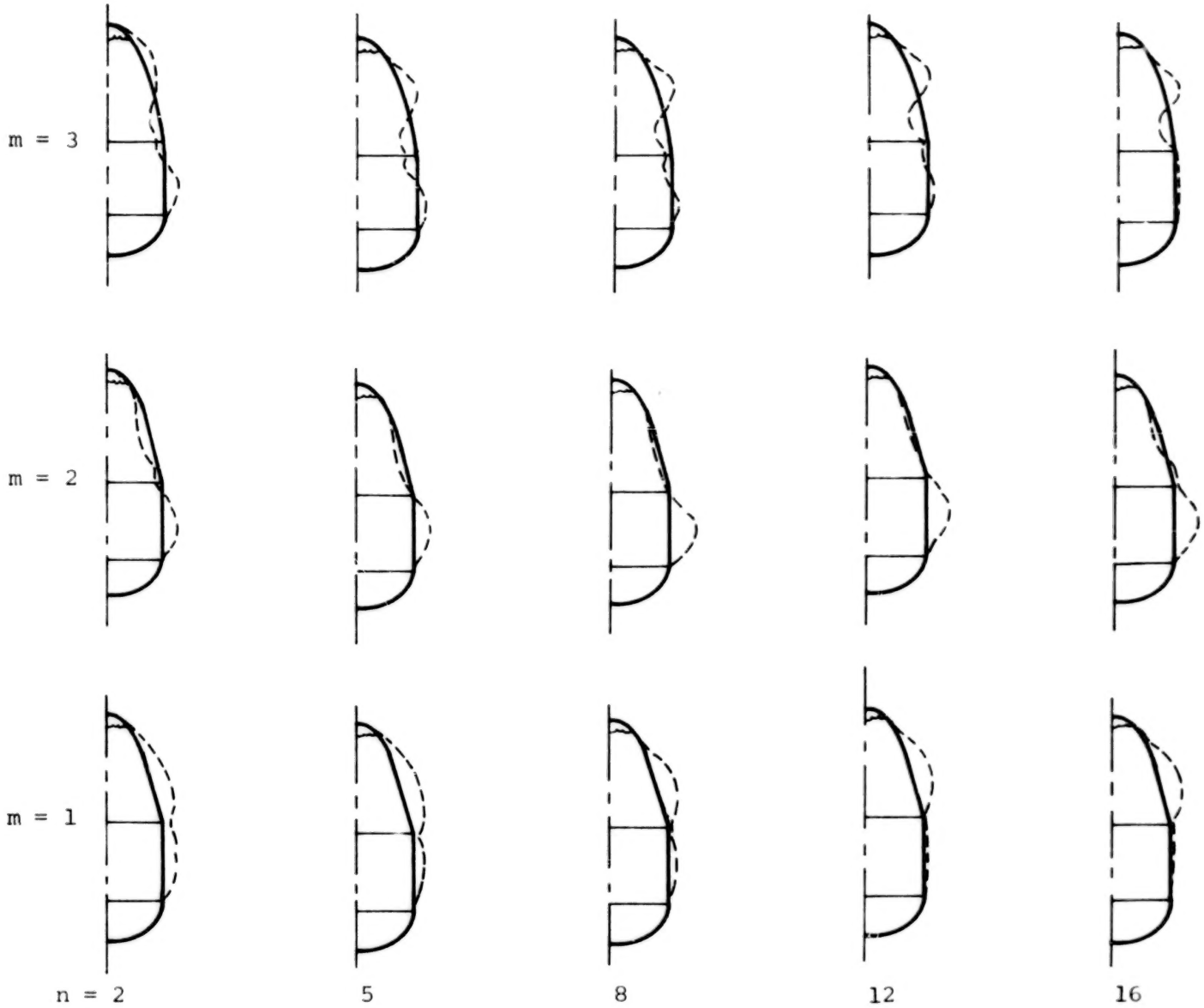

(b) Analytical meridional mode shapes.

Figure 5.- Concluded.

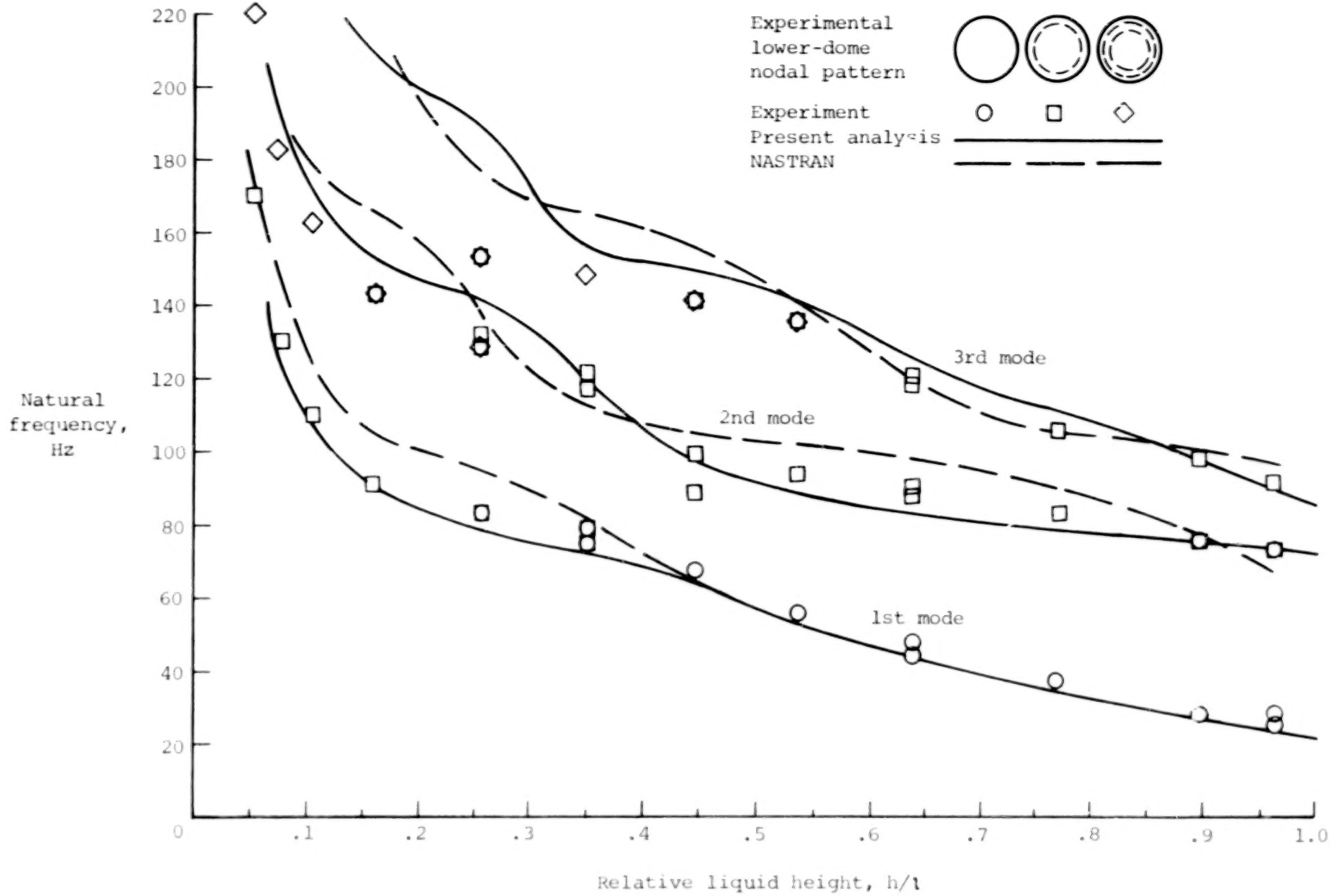

(a) Variation of natural frequency with liquid height.

Figure 6.- Axisymmetric (n = 0) vibration modes of propellant tank.

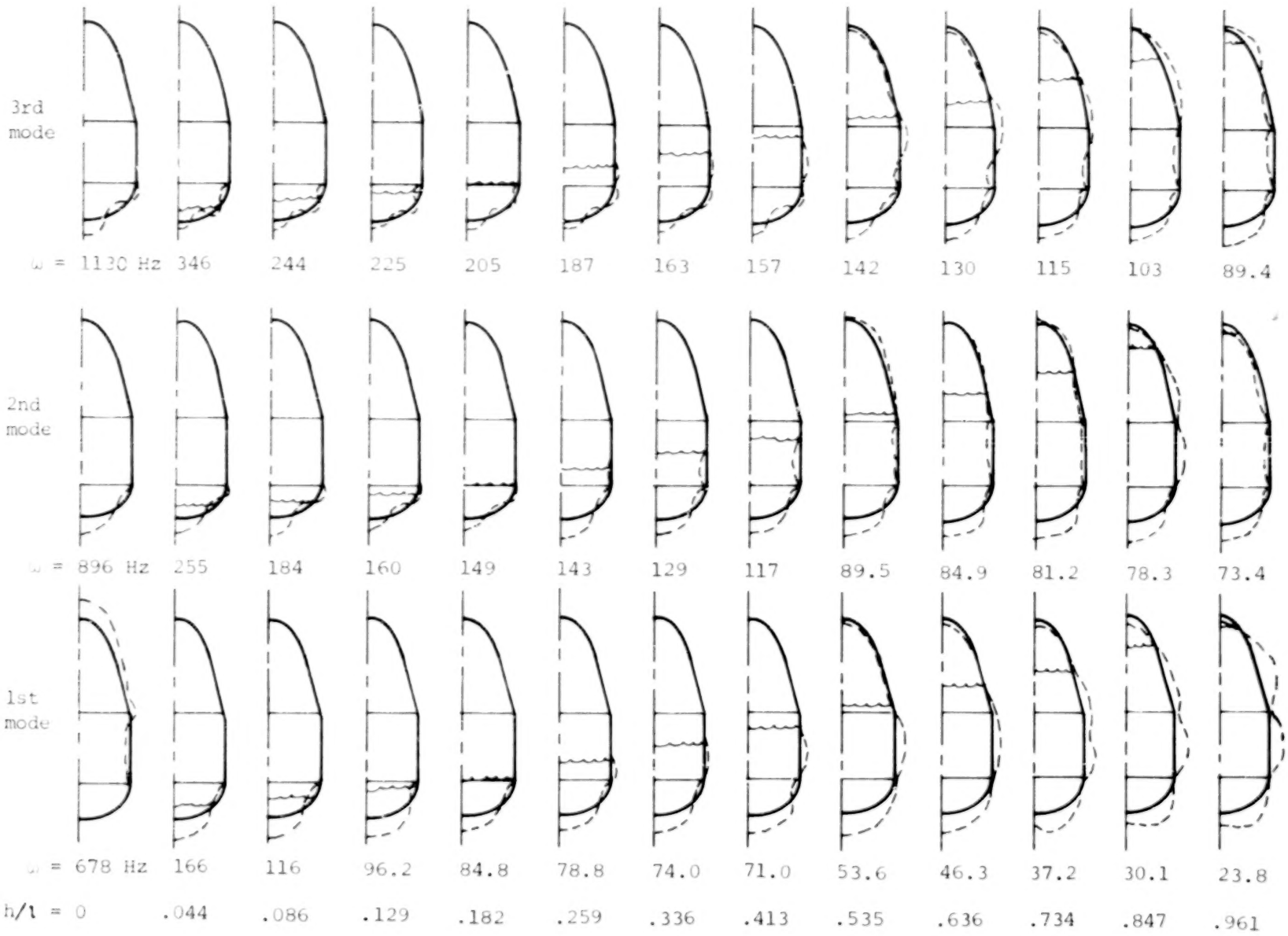

(b) Analytical meridional mode shapes and frequencies.

Figure 6.- Concluded.

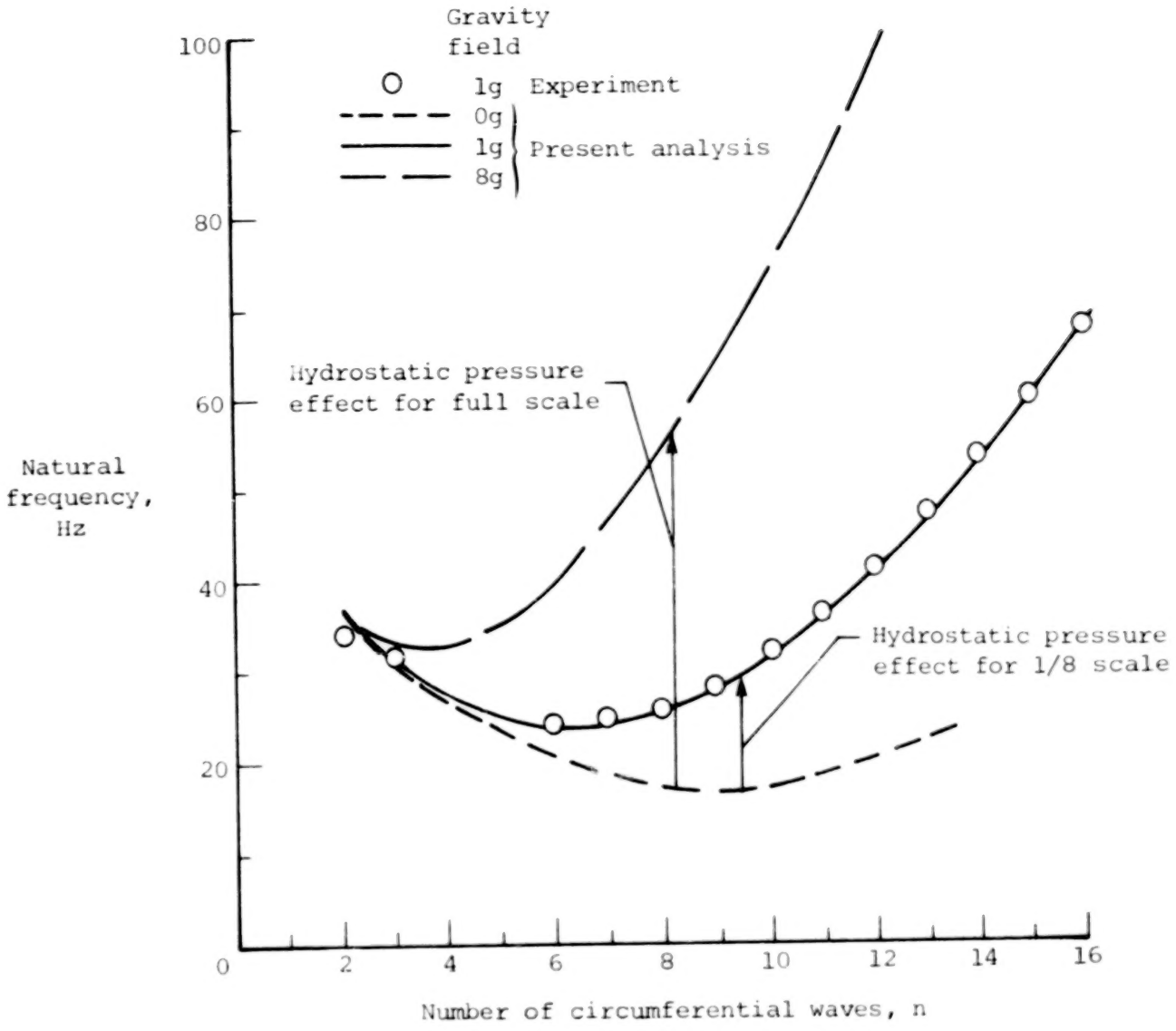

Figure 7.- Effect of hydrostatic pressure for 1/8-scale liquid-filled propellant tank and for full-scale equivalent. m = 1.

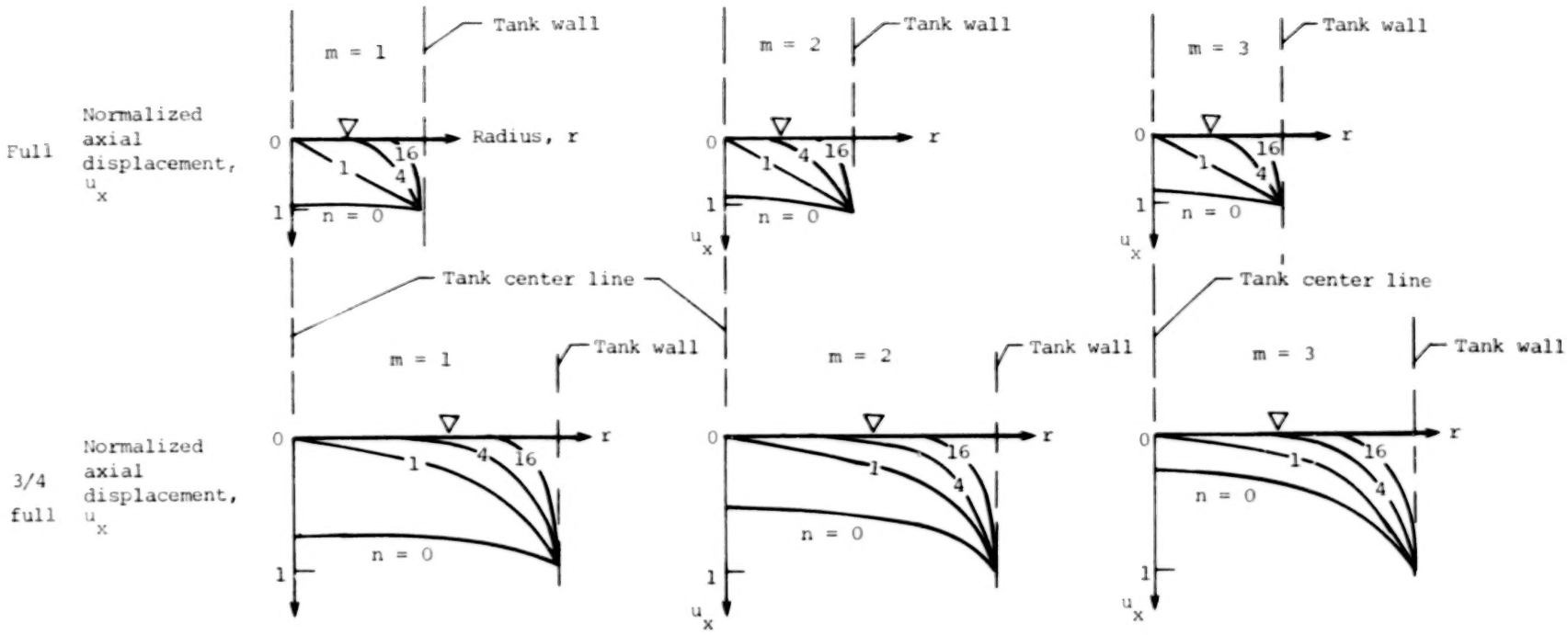

Figure 8.- Normalized axial displacements of free surface (denoted by ▽) for full and three-quarters full propellant tanks in first three meridional modes (m = 1,2,3).

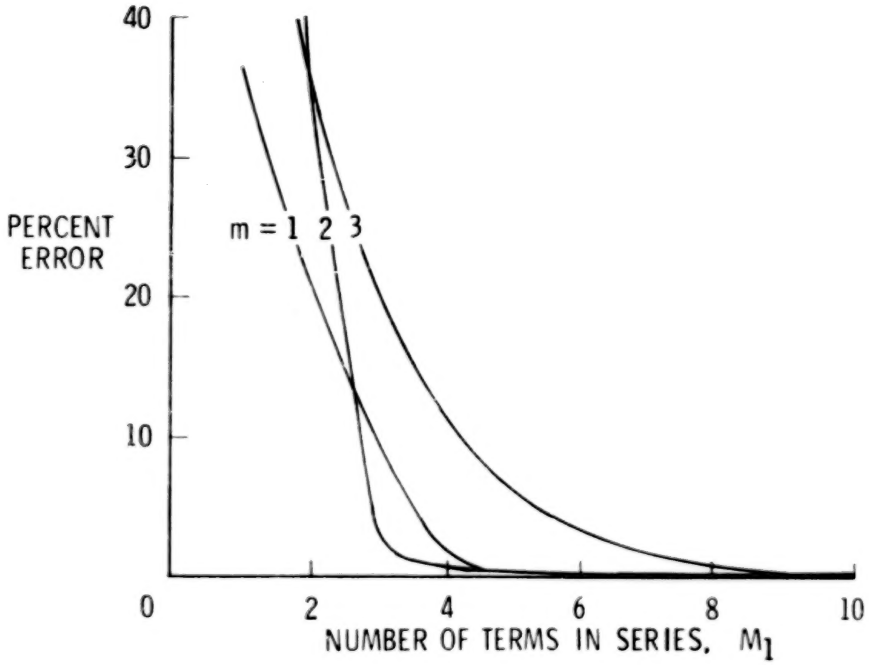

Figure 9.- Accuracy and convergence of predicted frequencies of first three meridional modes (m = 1,2,3) for full propellant tank. n = 6; $M_2 = M_3 = 0$.

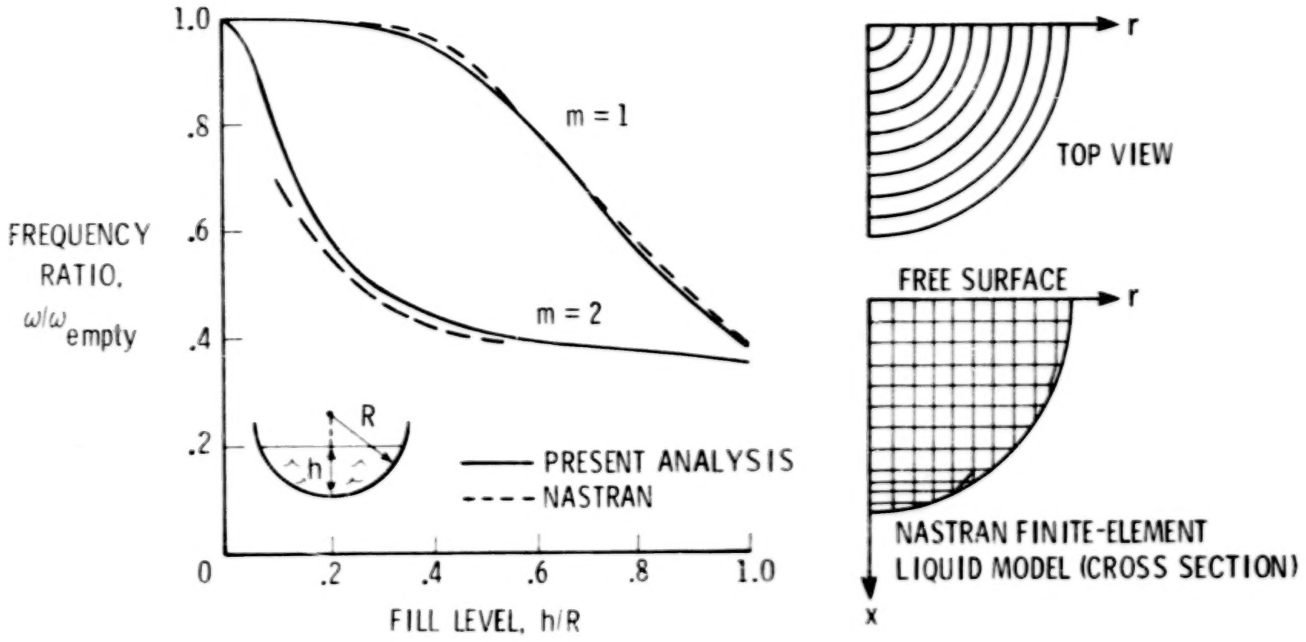

(a) Frequency ratio.

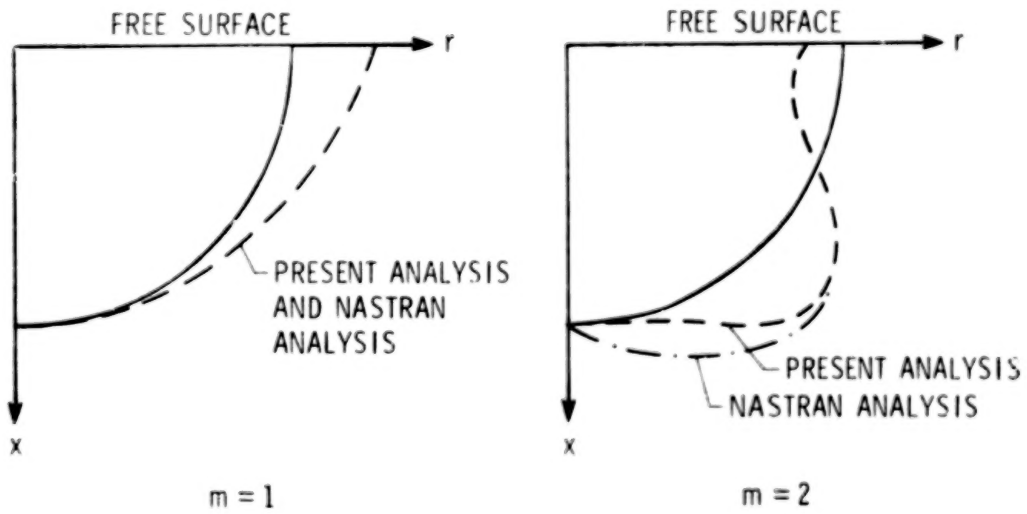

(b) Normal displacements of shell wall.

Figure 10.- Analytical vibration modes of water-filled aluminum hemisphere. n = 2; radius-to-thickness ratio = 100.

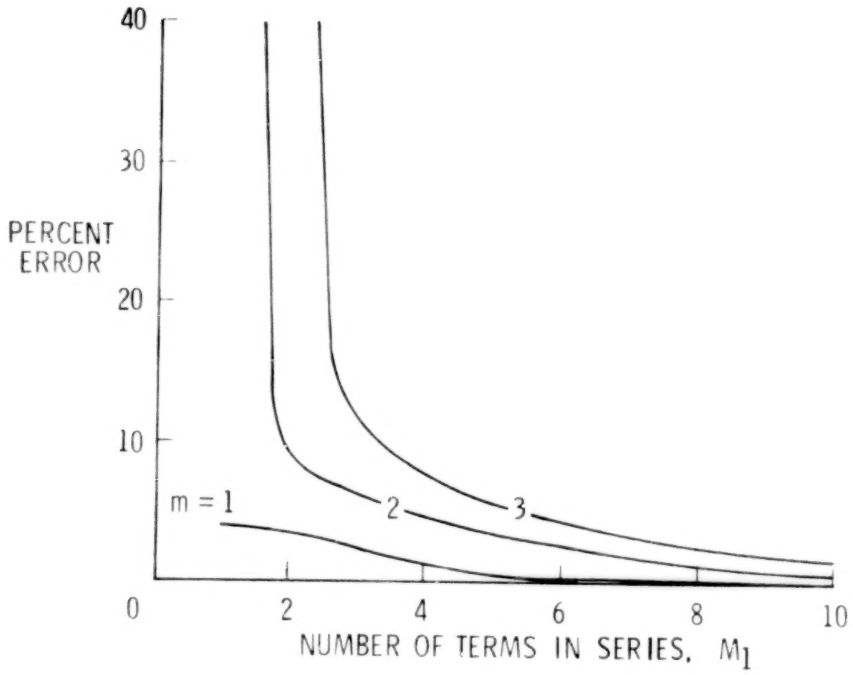

Figure 11.- Accuracy and convergence of predicted frequencies of first three meridional modes (m = 1,2,3) of full hemisphere. n = 2; $M_2 = M_3 = 0$.

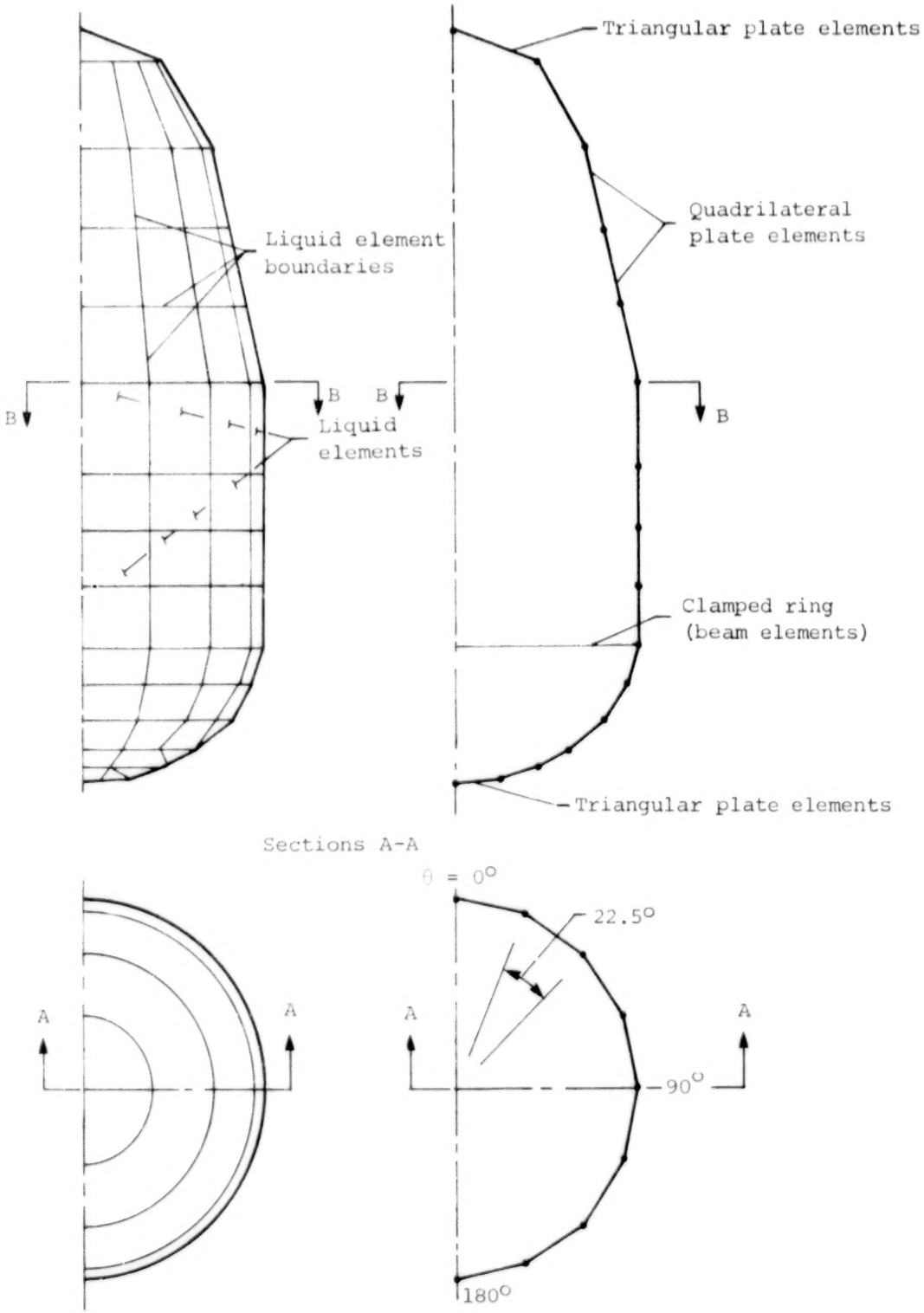

(a) Liquid model. (b) Structural model.

Figure 12.- NASTRAN models of half of propellant tank.

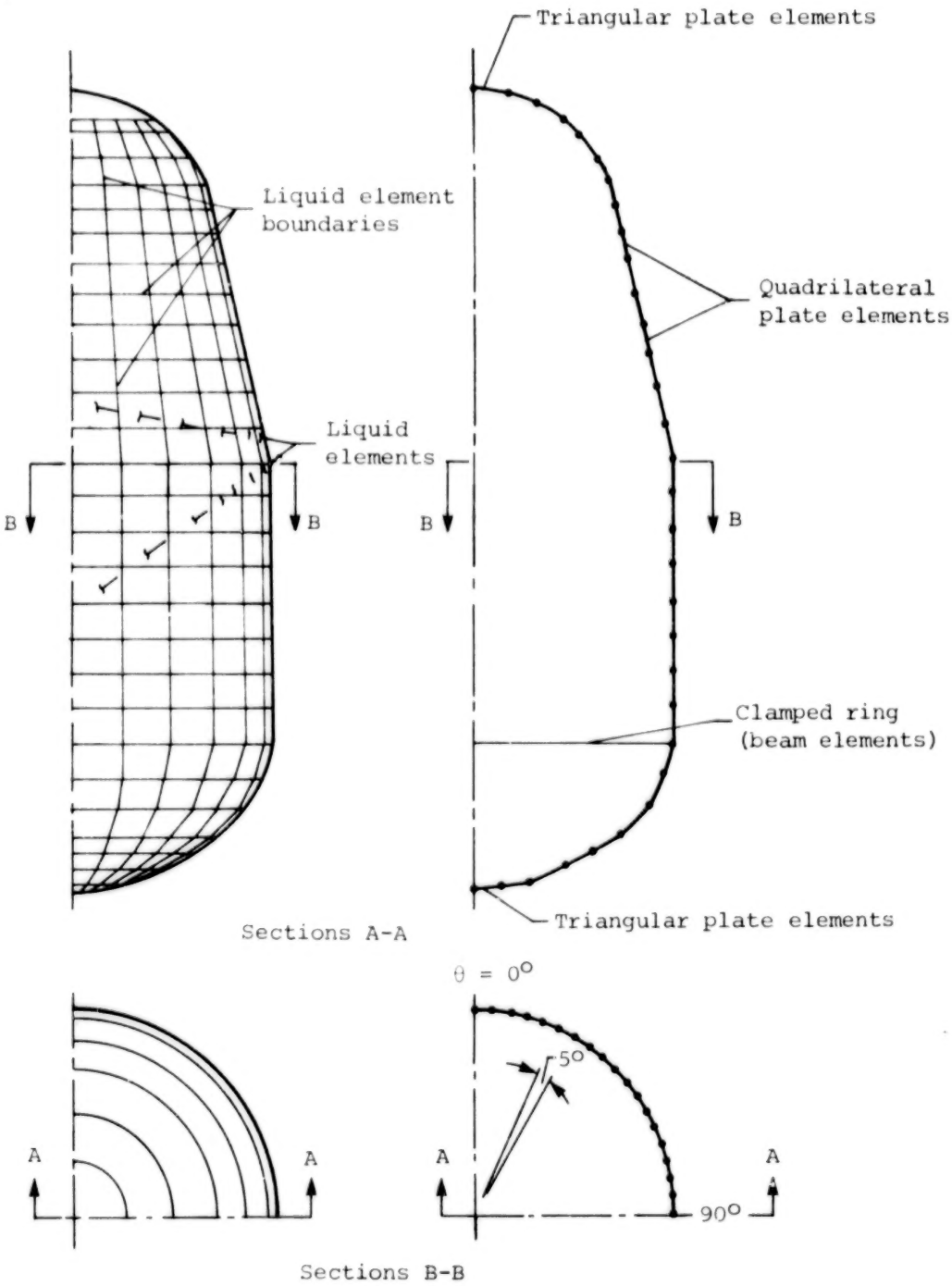

(a) Liquid model. (b) Structural model.

Figure 13.- Finer grid NASTRAN models of a quarter of prcpellant tank.

1. Report No.	2. Government Accession No.	3. Recipient's Catalog No.
NASA TP-1558		

4. Title and Subtitle	5. Report Date
HYDROELASTIC VIBRATION ANALYSIS OF PARTIALLY LIQUID-FILLED SHELLS USING A SERIES REPRESENTATION OF THE LIQUID	March 1980
	6. Performing Organization Code

7. Author(s)	8. Performing Organization Report No.
Jerrold M. Housner, Robert W. Herr, and John L. Sewall	L-13279
	10. Work Unit No. 506-53-53-03

9. Performing Organization Name and Address	11. Contract or Grant No.
NASA Langley Research Center Hampton, VA 23665	

12. Sponsoring Agency Name and Address	13. Type of Report and Period Covered
National Aeronautics and Space Administration Washington, DC 20546	Technical Paper
	14. Sponsoring Agency Code

15. Supplementary Notes

16. Abstract

A series representation of the oscillatory behavior of incompressible nonviscous liquids contained in partially filled elastic tanks is presented. By selecting each term of the series on the basis of the hydroelastic vibrations in circular cylindrical tanks, each term satisfies the governing liquid equation (Laplace's equation) but does not satisfy the liquid-tank interface compatibility. By using a complementary energy principle presented in this paper, the superposition of these terms is made to approximately satisfy the interface compatibility. This analysis is applied to the gravity sloshing and hydroelastic vibrations of liquids in hemispherical tanks and in a typical elastic aerospace propellant tank. With only a few series terms being retained, the results correlated very well with existing analytical results, NASTRAN-generated analytical results, and experimental test results. Hence, although each term is based on a cylindrical tank geometry, the superposition can be successfully applied to noncylindrical tanks.

17. Key Words (Suggested by Author(s))	18. Distribution Statement
Hydroelastic vibrations Liquid-shell interaction	Unclassified - Unlimited Subject Category 39

19. Security Classif. (of this report)	20. Security Classif. (of this page)	21. No. of Pages	22. Price*
Unclassified	Unclassified	65	$5.25

* For sale by the National Technical Information Service, Springfield, Virginia 22161

NASA-Langley, 1980